Nucleosynthesis with Tritium

Ani Aprahamian, R. James deBoer, Joachim Görres, Maxwell Q. Sorensen, and Michael Wiescher‡

The Joint Institute for Nuclear Astrophysics, Department of Physics and Astronomy, University of Notre Dame, Notre Dame, Indiana 46556 USA

E-mail: mwiesche@nd.edu, rdeboer1@nd.edu

Maria Gatu-Johnson

Plasma Science and Fusion Center, Massachusetts Institute of Technology, Cambridge, Massachusetts, 02139 USA

Chad J. Forrest and Arnold Schwemmlein

Laboratory for Laser Energetics, University of Rochester, Rochester, New York, 14623 USA

Abstract.

This paper reports on the possible role of tritium-induced reactions of light nuclei, which may influence nucleosynthesis in short-lived environments such as the third minute of the Big Bang. They may also play a role during the emergence of the neutrino-driven shock front in core collapse supernovae or merging neutron stars at extreme densities. The production of tritium requires a very dynamic and neutron-rich environment; under such conditions tritium-induced reactions are expected to play an important role in the development of specific reaction patterns that could lead to a delayed release of neutrons influencing the associated nucleosynthesis. Here, we summarize different possible reaction sequences and discuss the strength and impact of tritium cluster resonances that occur near the tritium threshold in the respective compound systems.

‡ Corresponding author.

1. Introduction

Tritium is a neutron-rich hydrogen isotope with a short half-life of 12.323 years. In general, tritium does not play a significant role in nucleosynthesis considerations, and therefore, the associated nuclear reactions have not been evaluated in detail by the nuclear astrophysics community. The naturally occurring tritium in air and water on earth is produced in small amounts by cosmic ray-induced reactions such as $^{14}\mathrm{N}(n,t)^{12}\mathrm{C}$, but, in long-lived stellar burning scenarios, tritium is usually not considered significant. However, there are a few short-lived nucleosynthesis scenarios in which tritium formation and tritium-induced reactions are critical and should not be neglected.

The first scenario is the onset of nucleosynthesis during the third to tenth minutes after the Big Bang, when primordial isotopes such as hydrogen (^{1}H), deuterium (^{2}H), tritium (^{3}H), ^{3}He, ^{4}He, and small amounts of ^{6}Li, ^{7}Li and ^{7}Be are produced. Nucleosynthesis towards heavier masses is constrained by the mass gaps at $A = 5$ and 8, which can be overcome by tritium-induced reactions [1, 2].

A second important site for tritium-induced reactions is associated with the reassembling of isotopes after the electron capture-induced core collapse of massive stars, while a third site includes the core conditions of two merging neutron stars. In these astrophysical scenarios with extreme temperatures and densities, all elements in the core are dissociated into protons, neutrons, and alphas, prior to the rebounce and subsequent expansion by neutrino-driven winds [3, 4]. The expansion and associated cooling leads to the reassembly of heavier nuclei in statistical equilibrium. This reassembling process is handicapped by the need for three particle interactions such as the triple-α and the $\alpha - \alpha - n$ processes, which are not in equilibrium, but could be by-passed by tritium induced reactions and tritium's capacity to store the neutrons for a time period before releasing them again in subsequent nuclear reaction processes. The time period is directly correlated with the associated reaction rates. We consider these processes and try to establish improved reaction rates on the basis of the available experimental data, taking into account all open channels. Our results are of interest for the nuclear astrophysics community but also far beyond for applications in high-intensity laser-driven acceleration techniques, for which new dynamical quantum calculations promise a considerable enhancement in fusion reactions due to laser-nucleus interactions at deep subbarrier energies [5].

2. Tritium in Big Bang Nucleosynthesis

Big Bang nucleosynthesis [1, 2] sets in with the $^1\mathrm{H}(n,\gamma)^2\mathrm{H}$ reaction, where tritium then forms by the subsequent, but considerably weaker, neutron capture process $^2\mathrm{H}(n,\gamma)^3\mathrm{H}$, or by deuterium fusion $^2\mathrm{H}(d,p)^3\mathrm{H}$, before being depleted by reaction processes induced by deuterium or α-particles [6]. A balance between the production and depletion reactions maintains the abundance of tritium until freeze-out occurs and the eventual β-decay or also (p,n) charge exchange conversions of tritium to ^{3}He. Tritium reaches

maximum abundances after the fifth minute, at a time when the rapid expansion of the Big Bang environment starts to inhibit any further nuclear reactions. The abundance predictions for tritium strongly depend on the tritium depletion rates of the ^{3}H(p,γ) and ^{3}H(d,n) reactions [7, 8]. The data rely largely on accelerator-based studies, but are presently also being studied at laser plasma facilities such as the National Ignition Facility (NIF) at Lawrence Livermore National Laboratory or at the Omega plasma fusion facility at the University of Rochester [9]. In addition to these reactions, more exotic fusion processes that emit two light particles may occur, such as ^{3}H$(t,2n)^4$He, a process that is dominated by tail contributions of higher energy resonances [10, 11]. The S-factor is essentially constant, and the reaction rate will increase exponentially with temperature.

A particularly important case is the ^{3}H$(\alpha,\gamma)^7$Li fusion reaction, where low energy data, $E_{\rm c.m.} \leq 0.4$ MeV show pronounced discrepancies [7]. This reaction is an important link for rapidly transferring the hydrogen isotope across the mass $A = 5$ gap into the lithium mass range and therefore can impact the solution to the "Li problem" in early universe abundance observations, where the predicted values of ^{7}Li seem to be three to four times higher than the observed values [12]. It is generally argued that the observed primordial ^{7}Li in the atmosphere of metal-poor stars is primarily produced by the electron capture decay of ^{7}Be [13] and possibly also via the ^{7}Be$(n,p)^7$Li charge exchange process [14, 15]. The different feeding mechanisms depend on a rather complex reaction pattern which also includes the ^{7}Be$(n,\alpha)^4$He link [16].

Although a recent analysis of lithium diffusion properties in old metal-poor stars has been suggested as a possible solution to the Li problem [17], the difference between observed and predicted Li abundances can also be reduced by tritium-induced depletion reactions on beryllium-7 [18] and lithium-7 directly produced via the aforementioned ^{3}H$(\alpha,\gamma)^7$Li reaction. Given the high abundances of tritium in the early Big Bang environment, the strength of the subsequent ^{7}Be+t and the^{7}Li+t reaction channels need to be investigated as possible reaction leaks, channeling material from ^{7}Be and ^{7}Li across the mass gap of $A = 8$, feeding the synthesis of the heavier isotopes. This process has been suggested as a potential solution for the lithium problem [19, 1].

2.1. ^{7}Be+t reaction channels

There are very limited data that provide information about the ^{7}Be+t fusion process. With a Q-value of 18.67 MeV, several reaction channels are open, ^{7}Be$(t,\gamma)^{10}$B, ^{7}Be$(t,n)^9$B, ^{7}Be$(t,p)^9$Be, ^{7}Be$(t,\alpha)^6$Li, and the charge exchange process ^{7}Be$(t,^3He)^7$Li. Through the inverse ^{7}Li$(^3He,t)^7$Be reaction, several broad resonance features at excitation energies above 18.8 MeV have been identified, which could feed all the listed reaction channels. While early studies argued for a direct reaction mechanism [20], subsequent measurements claimed the observation of rather broad resonances. In our analysis we concentrate on the contribution of known broad levels above 18.8 MeV. Most notable is a broad (1^-) state at about 20.1 MeV excitation energy that decays

directly into the triton channel [21], while the lower energy range exhibits resonances at 19.24 and 18.80 MeV with spin-parity assignments of 2^- and 2^+, respectively, that decay into other channels. However, there is no direct experimental information on the strength of the different decay channels and the strengths of the different channels have been estimated on the basis of the existing literature [20, 21]

2.2. ^{7}Li+t reaction channels

The strength of the $^7\mathrm{Li}(t,\gamma)^{10}\mathrm{Be}$ radiative capture process must be studied together with the competing $^7\mathrm{Li}(t,n)^9\mathrm{Be}$ fusion reaction, which is probably significantly stronger than the radiative capture of tritium. A recent R-matrix analysis of accelerator-based measurements [22, 23] seeks to explain the pronounced enhancement in the low-energy S-factor range of the $^7\mathrm{Li}(t,n)^9\mathrm{Be}$ reaction [24] by suggesting the existence of a low energy resonance. Some Big Bang nucleosynthesis simulations include these considerations and tritium-induced reaction processes have been added to reaction networks [1]. However, the reaction rates used in these network simulations were extracted from the `TALYS` statistical model reaction code [25]. This statistical model code is unreliable for light nuclei with low level densitites. The uncertainties in the results are not much better than previous estimates based on simple potential model estimates for reaction cross sections and reaction rates [26]. The reaction rates for tritium-inducted capture and fusion processes need to be revisited and measured experimentally to fully determine the impact of tritium in the early universe environments.

3. Tritium at the Onset of the Supernova Shock

Supernova core collapse dissociates the abundance distribution in the core of a pre-supernova star in nuclear statistical equilibrium to its baryonic entities, protons, neutrons, and α-cluster remnants. These particles are embedded in a sea of leptonic matter [3]. With the expansion of the shock, driven by the re-bounce and neutrino wind pressure [27], the isotopes reassemble in nuclear statistical equilibrium (NSE) [28], where the mass fractions X_i of all nuclei with charge number Z_i and neutron number N_i in NSE can be expressed in terms of the chemical potentials μ_p of the protons and μ_n of the neutrons, respectively, the partition function G_i determining the impact of thermally excited states as well as their nuclear binding energies Q_i

$$Q_i = (Z_i m_p + N_i m_n - m_i)c^2, \tag{1}$$

as defined in terms of the masses of protons m_p, neutrons m_n, nuclei m_i and

$$X_i = \frac{\rho_i}{\rho} G_i \left(\frac{2\pi m_i kT}{h^2}\right)^{3/2} \exp \frac{Z_i\mu_p + N_i\mu_n + Q_i}{kT}, \tag{2}$$

where ρ is the density of the nuclear matter and ρ_i the density of isotope i .

However, rapid recombination towards the α-chain is handicapped by the mass $A = 5$ and 8 gaps, which must be bridged in order to process toward heavier isotopes.

The bridge is expected to be formed through three particle processes. This is in particular the triple-α-process $^4\mathrm{He}(2\alpha,\gamma)^{12}\mathrm{C}$ fusion reaction where three α-particles fuse to make ^{12}C. In the case of environments with a high neutron density, the $^4\mathrm{He}(\alpha n,\gamma)^9\mathrm{Be}$ and the $^4\mathrm{He}(nn,\gamma)^6\mathrm{He}$ reactions [29] will also contribute by bridging the gaps through fast neutron-induced reaction processes unhindered by the Coulomb barrier; this may drive the reaction path towards the neutron-rich side of stability and trigger a light r-process [30, 31]. In addition to these processes involving the capture of α-particles and neutrons by ^{4}He, the sequential capture of two neutrons by hydrogen, or more efficiently a single neutron capture followed by the $^2\mathrm{H}(d,p)$ reaction, may also form tritium in large amounts, which can reach abundances higher than α-particles and free protons [32]. Possible implications of tritium-induced reactions in a rapidly expanding supernova shock front environment are not yet fully studied, but may provide a new path for rapidly forming light isotopes along the α-chain, to initiate a new light r-process path via the $^4\mathrm{He}(t,\gamma)^7\mathrm{Li}(n,\gamma)^8\mathrm{Li}$ reaction sequence with a variety of subsequent α-particle or neutron capture reactions [33]. In this context, tritium interactions with light halo nuclei such as the $^6\mathrm{He}(t,n)^8\mathrm{Li}$ and $^8\mathrm{Li}(t,n)^{10}\mathrm{Be}$ reactions may also play a significant role and hence be of interest. These reactions need to be studied in inverse kinematics with short-lived ^{6}He and ^{8}Li beams using tritium implanted targets. Similar studies have been conducted using deuterated targets to explore the role of the $^8\mathrm{Li}(n,\gamma)^9\mathrm{Li}$ reaction [34].

Synthesis reactions upon reaching the strong neutron source via the $^9\mathrm{Be}(\alpha,n)^{12}\mathrm{C}$ reaction, tritium induced reactions on ^{9}Be, such as $^9\mathrm{Be}(t,\gamma)^{12}\mathrm{B}$, $^9\mathrm{Be}(t,n)^{11}\mathrm{B}$, $^9\mathrm{Be}(t,d)^{10}\mathrm{B}$, and $^9\mathrm{Be}(t,\alpha)^8\mathrm{Li}$, might also feed neutron-rich light nuclei as additional seeds for driving a light r-process. Earlier studies of tritium-induced radiative capture reactions on heavier nuclei include $^{12}\mathrm{C}(t,\gamma)^{15}\mathrm{N}$, suggesting pronounced resonant features [35]. Other reaction channels, such as the $^{12}\mathrm{C}(t,n)^{14}\mathrm{N}$ and $^{12}\mathrm{C}(t,p)^{14}\mathrm{C}$ reactions, also need to be investigated over a broad range of energies, as earlier studies suggest a complex configuration of broad resonances [36]. Tritium-induced reactions will potentially have a significant impact on the reaction network, releasing fresh neutrons and initiating an r-process reaction flow even in the low mass range.

Figure 1 shows the main tritium and α-induced reaction paths that bridge the mass $A = 5$ and $A = 8$ gaps, facilitating the production of CNO isotopes.

3.1. Tritium as neutron storage and neutron source

Free neutrons are quickly absorbed in radiative neutron capture reactions on light isotopes with high abundances, typically labeled neutron poisons, or on heavier isotopes in the framework of the s-process [37]. In explosive environments such as the neutrino wind driven shockfront of a supernova, neutrons are quickly absorbed by heavy radioactive species as part of the light r-process [38]. The neutrons facilitate the build-up of heavier elements. Additional neutron production in such an environment is indeed possible through (α,n) reactions on light nuclei [39, 40].

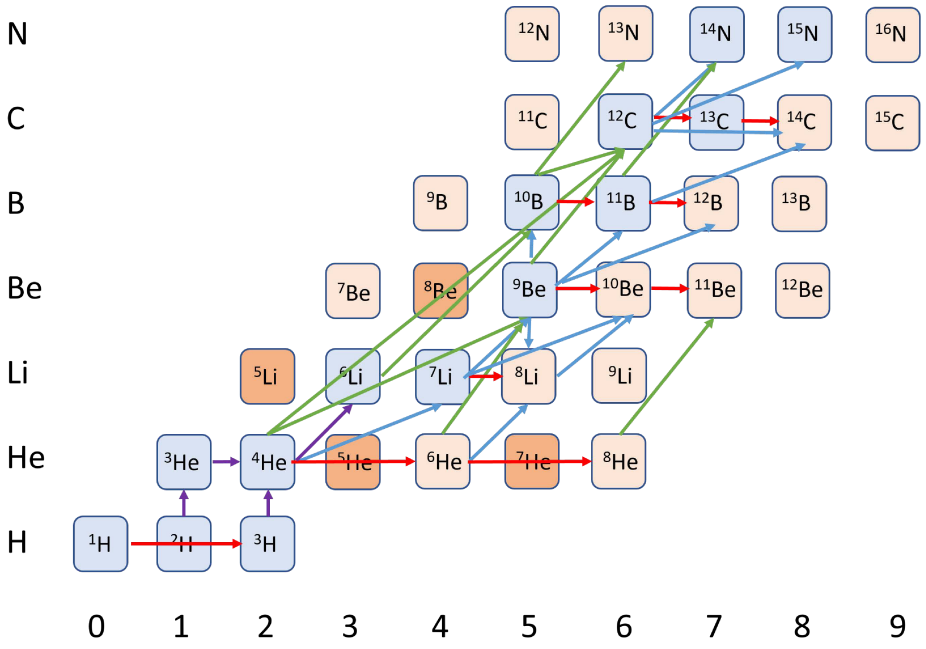

Figure 1. The most important tritium (blue lines) and α-particle (green lines) induced reactions bridging the mass 5 and 8 gaps between the light nuclei and those in the CNO range. Also shown in red are important neutron capture reactions in that mass range and, in purple, important deuteron capture reactions. Stable nuclei are marked in blue, particle unstable nuclei in red, and beta-unstable nuclei in rose.

Neutron storage in tritium plays an interesting role for storing neutrons, which may be later released via (t, n) resonant stripping processes at low energies. The release time τ is the time difference between the neutron induced processes producing tritium and subsequent neutron release via tritium induced (t, n) reactions. The subsequent release time τ_i is inversely proportional to the (t, n) reaction rate as well as the density of the stellar environment and the abundance of the reaction partners $N_i = X_i/A_i$ expressed in terms of their respective mass fraction X_i and mass number A_i

$$\tau_i = \frac{A_i}{X_i} \cdot \frac{1}{(\rho \cdot N_A \langle \sigma \mathrm{v} \rangle)}. \tag{3}$$

These lifetimes depend critically on the density conditions in the stellar environment but more so on the temperature dependent reaction rates $N_A\langle\sigma\mathrm{v}\rangle$, which will be discussed in the next chapter for the different triton induced processes. Based on the strength of the reaction rates, neutrons can be stored for considerable amounts of time before being released again, influencing subsequent nucleosynthesis patterns. This is an important feature in rapid nucleosynthesis processes, since neutrons can not only be released in (α, n) processes as suggested by [39, 40] but also in (t, n) processes as presented here, enhancing neutron flux and neutron-induced reaction patterns. Neutrons stored in tritium may provide a strong but delayed neutron flux to build heavier elements. In the following, we review and evaluate the reaction rates presently used for triton-induced reaction processes.

4. Tritium induced reactions on light isotopes

In this section, we seek to evaluate some of the tritium-induced reaction processes that can play a pivotal role in bridging the mass $A = 5$ and mass 8 gaps in the aforementioned scenarios. The reaction rates are temperature dependent functions, which are determined by the Maxwell-Boltzmann distribution of the interacting particles and the reaction probability or reaction cross sections $\sigma(E)_{t,A}$ between two charged particles, in our case tritium t and a second target particle A. For charged particle reactions, the cross sections are determined by the penetrability through the Coulomb barrier and decline exponentially with energy. For this reason, the energy-dependent cross section at a certain energy E, $\sigma(E)$ is often replaced by the astrophysical $S(E)$-factor, which is defined by the following expression:

$$S(E) = E\,\sigma(E)\,e^{2\pi\eta}. \tag{4}$$

In first approximation, this equation corrects the cross section for the tunneling penetrability through the Coulomb barrier. When written in terms of the $S(E)$-factor, the thermonuclear reaction rates per particle pair for $t + A$ can be described by the following expression:

$$\langle\sigma v\rangle_{t,A} = \left(\frac{8}{\pi\mu_{tA}}\right)^{1/2} \frac{1}{(kT)^{3/2}} \int_0^\infty S(E) \exp\left[-\frac{E}{kT} - 2\pi\eta\right] dE. \tag{5}$$

The parameter η approximates the impact of the Coulomb barrier and is defined as $\eta = (\mu_{tA}/2E)^{1/2} e^2 Z_t Z_A/\hbar$ with μ_{tA} as reduced mass of the reaction system in atomic mass units.

In the following, we convert the experimentally observed cross section data $\sigma(E)_{t,A}$ into $S(E)$-factor functions using Eq. (4) for better presentation and discussion. For most of the systems discussed here, the $S(E)$ factor represents a smooth function that can be easily implemented in Eq. (5).

4.1. Tritium induced radiative capture processes: $^3H(t,\gamma)^6He$, $^3He(t,\gamma)^6Li$, and $^3H(\alpha,\gamma)^7Li$

The first set of reactions to be discussed are the reactions between tritium and light nuclei $Z_A \leq 2$. These reactions are important since they provide the break-out links across the $A = 5$ mass gap.

Fig. 2 shows the mirror nuclei ^{6}He and ^{6}Li as compound systems for the ^{3}H+^{3}H and the ^{3}H+^{3}He fusion processes, respectively. Information on the level densities and high-energy excited states near the tritium threshold is limited and is mostly based on decades-old accelerator-based experimental studies. The missing states may enhance the $S(E)$-factor with significantly larger cross sections resulting from the resonances.

These tritium-induced radiative capture or fusion reactions would bridge the $A = 5$ mass gap and may eventually feed ^{6}Li, unless subsequent $^6\mathrm{Li}(p,\alpha)$ reactions facilitate

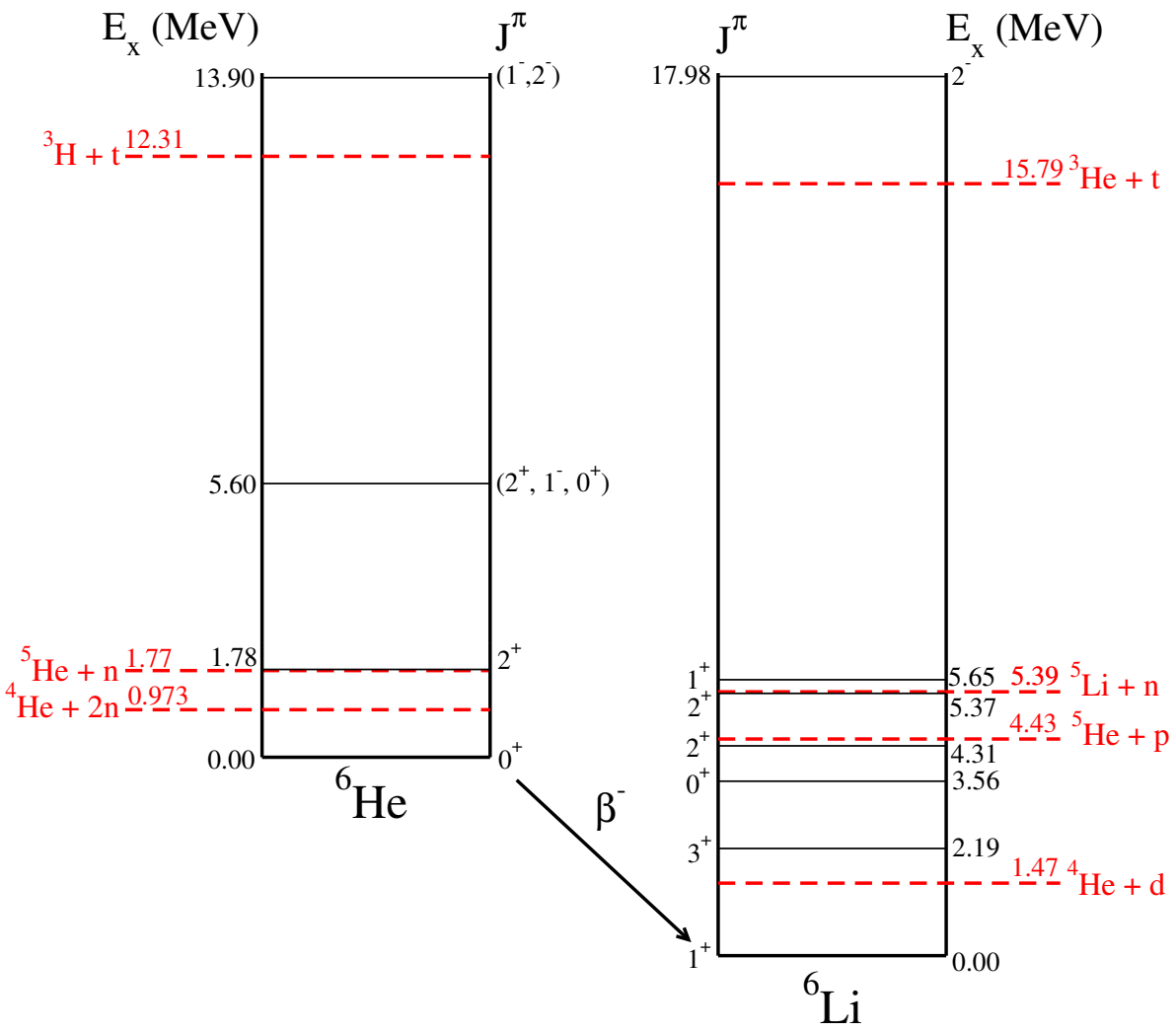

Figure 2. The known level structure of the ^{6}He and ^{6}Li mirror systems up to just above the ^{3}H+t and ^{3}He+t separation energies, respectively. Information about resonances near the tritium threshold is limited but it is expected that these neutron unbound resonances must be broad.

rapid conversion back to ^{3}He . The compound nuclei, ^{6}He and ^{6}Li, are produced at high excitation energies, but the level density information is sparse. The $^3\mathrm{H}(t,2n)^4\mathrm{He}$ process is non-resonant [41] and is expected to be substantially stronger than the competing direct radiative capture process $^3\mathrm{H}(t,\gamma)^6\mathrm{He}$ feeding the ground state of ^{6}He. Considering the relatively long half-life of ^{6}He, $T_{1/2} = 807.25$ ms [42], a subsequent nuclear reaction on these seed abundances might be possible.

Figure 3 shows the existing reaction data and R-matrix calculations for $^3\mathrm{H}(t,2n)^4\mathrm{He}$ and the radiative capture reaction $^3\mathrm{H}(t,\gamma)^6\mathrm{Li}$ calculated using the code `JEZEBEL`. The S-factor for the $E2$ radiative capture process of $^3\mathrm{H}(t,\gamma)^6\mathrm{He}$ is based on the electromagnetic interaction and is considerably lower than the experimental $S(E)$-factor for $^3\mathrm{H}(t,2n)^4\mathrm{He}$.

The comparison between the two branches suggests a small $\leq 0.001\%$ branch of the material to ^{6}He as a seed for subsequent processes such as the $^6\mathrm{He}(\alpha,n)^9\mathrm{Be}$ reaction that

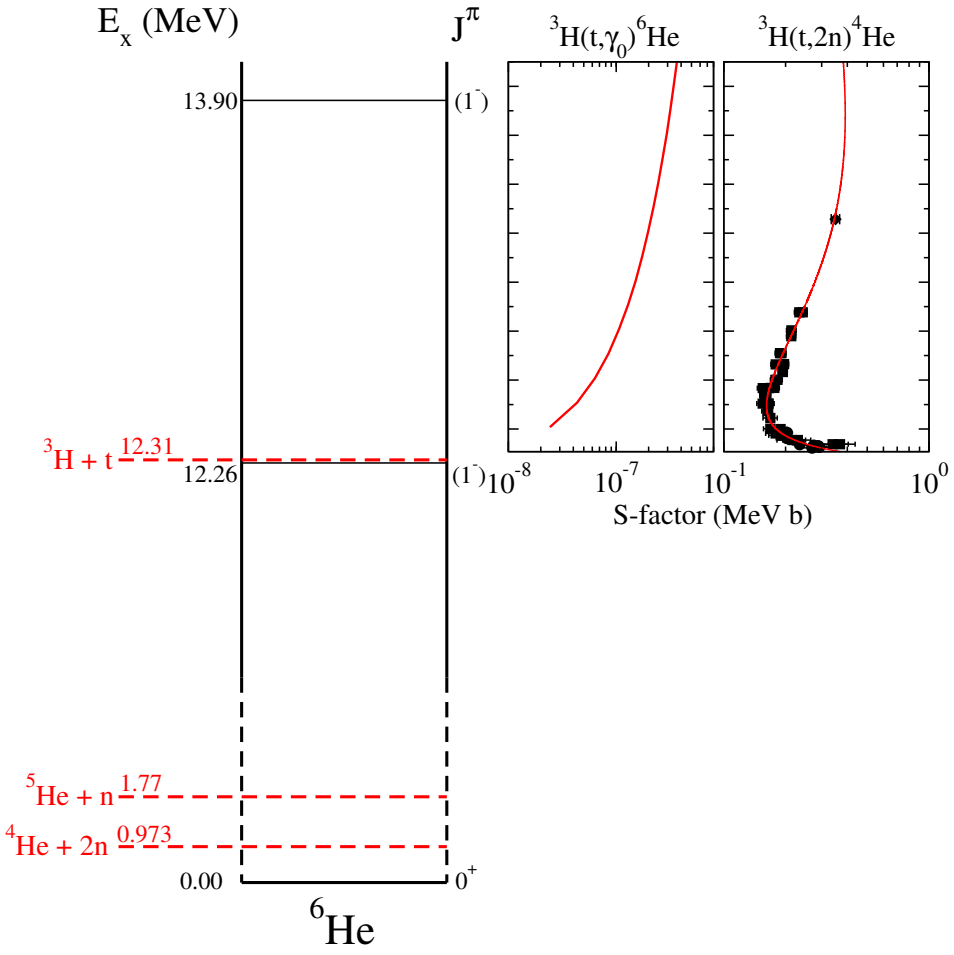

Figure 3. Level scheme for the ^{6}He system relevant to ^{3}H+^{3}H. The $S(E)$ factor for the ^{3}H$(t,2n)^4$He reaction at low energies has been measured by Govorov et al. [43], Serov et al. [44] and Jarmie and Allen [45]. A good description of the energy dependence was obtained using a two-level R-matrix fit made up of a subthreshold state and a higher energy one of the same J^π. A direct capture calculation (solid red curve) of the competing ^{3}H$(t,\gamma)^6$He reaction is also shown, where $E2$ multipolarity makes up about $\approx$90% of the amplitude with $M1$ the remaining $\approx$10%.

might bridge the $A = 8$ mass gap and thus facilitate the production of CNO isotopes. Feeding a small fraction of ^{6}He might also open a reaction channel towards the drip line via the ^{6}He$(t,n)^8$Li reaction, or merge closer to the line of stability with the ^{6}He$(p,\gamma)^7$Li reaction, unless the di-neutron capture reaction ^{6}He$(2n,\gamma)^8$He plays a major role [29]. Most of these reaction cross-sections are unknown, but they are most likely dominated by broad, yet unmeasured, resonances, and may be an interesting goal for experimental study with light or radioactive beams on a long-lived tritium target.

Also, for the compound nucleus ^{6}Li, proton, neutron, and deuterium channels are open at the threshold and will dominate the rapid depletion via ^{3}He$(t,p)^5$He$(n)^4$He, ^{3}He$(t,n)^5$Li$(p)^4$He, and ^{3}He$(t,d)^4$He, respectively. Radiative capture studies suggest a strong direct capture component to the ground state and the first excited states in the ^{3}He$(t,\gamma)^6$Li reaction branch [46]. The fusion mechanism toward higher energies is

facilitated through broad and interfering neutron unbound resonance states near the tritium threshold, with the width clearly dominated by the neutron partial widths. Towards higher energies, we expect broad and overlapping resonances to dominate the cross sections [47].

Considering the ^{3}He$(t,n)^5$Li reaction, the experimental data at low energies suggest a non resonant cross section, which could be matched by a two-nucleon-transfer distorted-wave Born-wave approximation calculation, however the potential parameters used do not reproduce the published elastic scattering data at somewhat higher energies [48]. Figure 4 shows the existing cross section data for the two ^{3}He$(t,n)^5$Li and ^{3}He$(t,\gamma)^6$Li reaction channels in the energy range between 0.5 and 2.0 MeV center of mass energy as well as an R-matrix fit to the data based on the limited experimental information available. The comparison shows that the radiative (t,γ) triton capture, based on the electromagnetic interaction Hamiltonian, is about two orders of magnitude smaller than the competing strong interaction based (t,n) deuteron stripping process.

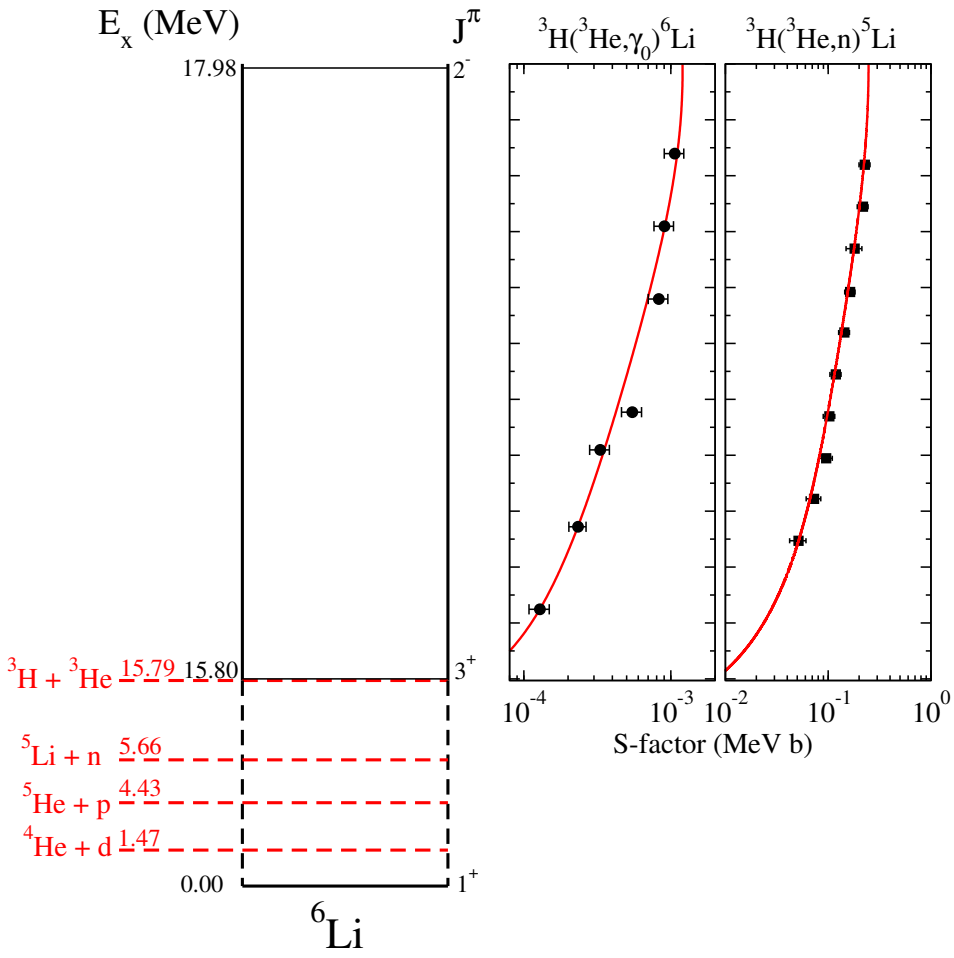

Figure 4. Level scheme of ^{6}Li near the tritium separation energy. Fusion cross sections were calculated with a two-level R-matrix simulation for the ^{3}H$(^3$He$,n)^5$Li and ^{3}H$(^3$He$,\gamma)^6$Li reactions at low energies and compared with the experimental data of Klopcic and Darden [48] and Blatt et al. [46], respectively.

For the $^3\mathrm{H}(\alpha,\gamma)^7\mathrm{Li}$ reaction, the Q-value is low and the compound nucleus ^{7}Li is produced at a low excitation energy of 2.467 MeV where only γ-decay to the ground state and the first excited state at 4.7761 MeV in ^{7}Li is possible [49]. The cross section for these two transitions is characterized by $s \rightarrow p$ direct capture process. This pattern is in good agreement with the mechanism of the mirror reaction $^3\mathrm{He}(\alpha,\gamma)^7\mathrm{Be}$, which plays a crucial part for the solar neutrino budget. Theoretical models describe the non-resonant reaction patterns for both reactions quite well [50]. Figure 5 shows the level structure of the compound nucleus ^{7}Li as well as the existing S-factor data for the fusion reaction, also shown is a fit to the data using `AZURE2`.

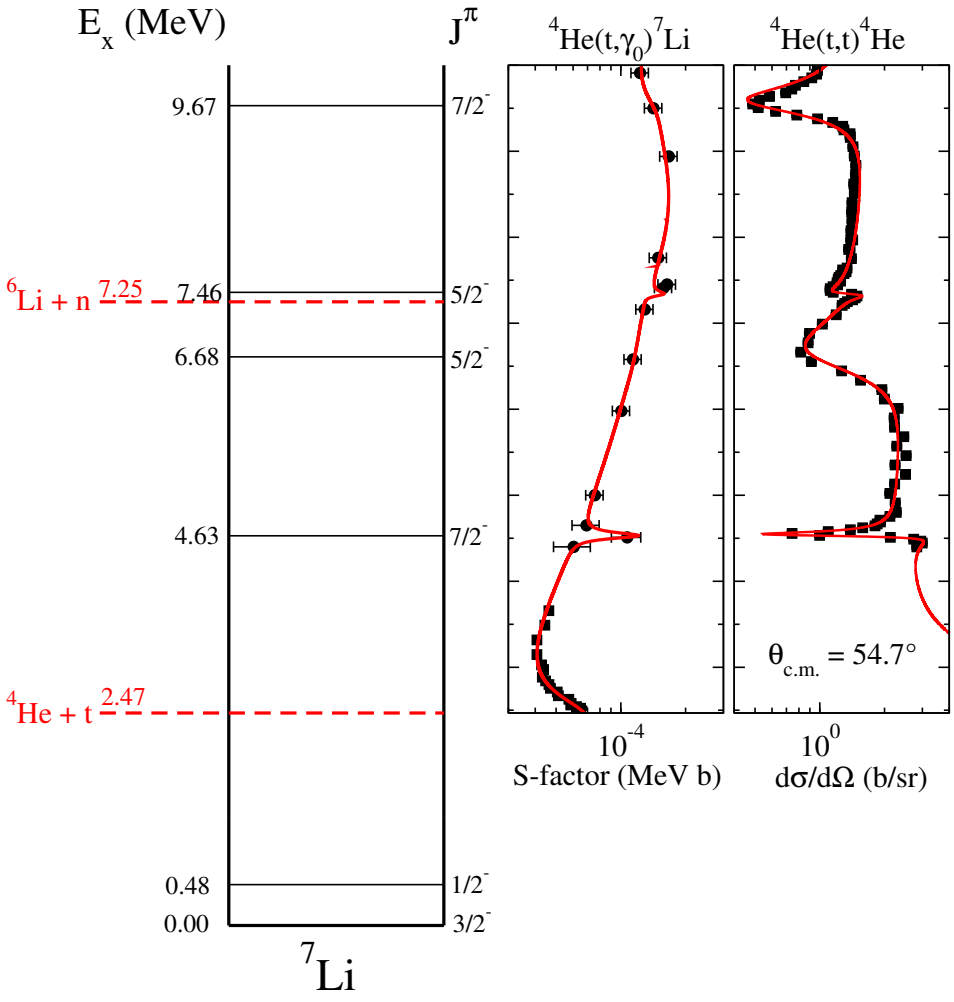

Figure 5. ^{7}Li level scheme, $^3\mathrm{H}(\alpha,\gamma)^7\mathrm{Li}$ S-factor [49, 51] and elastic scattering differential cross section [52] data.

All of these reactions have positive Q-values, promising a rather complex reaction network that bridges the mass gap at $A = 5$ during the third minute of the expanding universe, possibly impacting the production of $A = 6$ and $A = 7$ nuclei. They also will contribute to the reaction flow at the on-set of re-assembling more complex baryonic matter in the emerging shock front of core collapse supernovae and merging neutron

stars. Not considered in this context are neutrino induced processes, such as the ν induced reactions, which may drive weak interaction based the νp process [53, 54].

4.2. Tritium capture on heavier nuclei $A \geq 6$

While tritium capture reactions on hydrogen and helium isotopes may play a role in bridging the $A = 5$ gap, tritium capture on heavier isotopes may facilitate the bridging of the $A = 8$ gap as well, and need to be investigated in more detail. The Q-values of the reactions are rather high so that the respective compound nuclei are populated at high excitation energies. This translates into fairly high-level densities even for these low-mass compound nuclei. Indeed, the existing experimental results indicate broad cluster resonance structures dominating the reaction cross section at low tritium energies. However, these data lack detail and the absence of reliable structure information handicaps a reliable R-matrix analysis. The derivation of the here discussed tritium induced reactions relies on R-matrix calculations using `AZURE2` based on existing reaction data. In some cases the rate calculations are complemented by a statistical model analysis using the code `TALYS` [25].

4.2.1. Tritium on ^{6}He: $^6He(t,n)^8Li$ This reaction has a Q-value of 3.525 MeV with the tritium separation energy at 7.59 MeV. The reaction populates excited states in the ^{9}Li compound system. Only limited experimental information is available for levels over this excitation energy range [55], but three-triton cluster configurations are anticipated [56], which may increase three-triton fusion like the triple-alpha process, although that seems possible only if ^{6}He develops a large equilibrium abundance through the aforementioned $t + t$ fusion mechanism. This, however, is unlikely because of the very high tritium threshold in ^{6}He and parallels between a triple-alpha and a triple-triton process are not given.

Since the neutron threshold is open, a few broad and overlapping resonances are also anticipated in the ^{6}He$(t,n)^8$Li process. In fact, recent studies identified two tritium cluster configurations: one at 9.8 MeV with a total width of 1.7 ± 1.1 MeV corresponding to $3/2^-$ spin-parity, and a second one at 12.8 MeV was suggested to have $J^\pi = 7/2^-$ [57] . The width of the second states was not clearly identified but seems to be in the MeV range as well. An estimate of the cross section, based on recent data is presented in an R-matrix calculation, shown in Figure 6. Because the two cluster components ^{6}He and ^{3}H are neutron-rich, the cluster configuration in ^{9}Li might decay by two neutron emission ^{6}He$(t,2n)^7$Li, however due to the associated uncertainties a reliable estimate is not possible. More experimental studies are necessary to explore the detailed resonance features toward a more reliable R-matrix analysis.

4.2.2. Tritium capture on ^7Be There are no direct experimental data on the ^{7}Be+t fusion process; this would require reaction studies with two long-lived radioactive species. With a Q-value of 18.67 MeV, several reaction channels are open such as

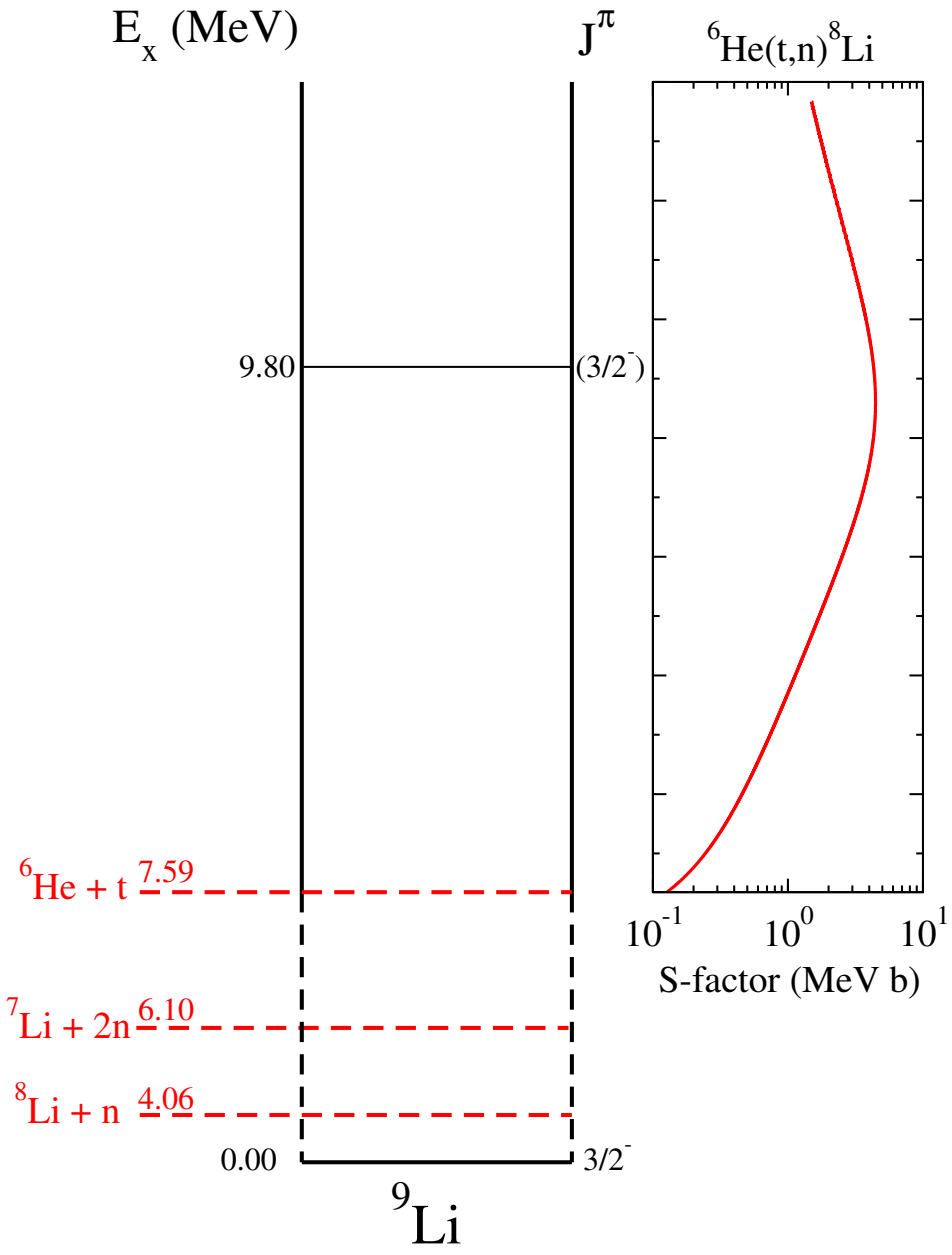

Figure 6. Level scheme of the ^{9}Li system near the triton separation energy. Very little experimental information is available. An R-matrix estimate of the S-factor is shown using the level parameters for the 9.8 MeV state reported by Ma et al. [57]. The contribution of the higher energy state at 12.8 MeV is negligible.

^{7}Be$(t,\gamma)^{10}$B, ^{7}Be$(t,n)^9$B, ^{7}Be$(t,p)^9$Be, ^{7}Be$(t,\alpha)^6$Li, and the charge exchange process ^{7}Be$(t,^3He)^7$Li. Based on the available nuclear structure and reaction data, several broad resonances have been identified at 18.80 MeV with $\Gamma \approx$500 keV, at 19.24 MeV with $\Gamma = 190 \pm 20$ keV, with spin-parity assignments of 2^+ and 2^-, respectively, as well as the 1^- state at about 20.1 MeV excitation energy with a total width of $\Gamma = 350 \pm 70$ keV.

Although there is no direct experimental information on the partial widths of

the different decay channels, the strengths have been estimated based on the existing literature on the strength of the reaction channels associated with the compound nucleus ^{10}B in the energy range above 18.7 MeV [20, 21, 58, 59] to perform an R-matrix calculation for the ^{7}Be$(t,^{3}He)^{7}$Li and ^{7}Be$(t,n)^{9}$B reactions using the multichannel code `AZURE2`. The results are shown in Fig. 7. All ^{7}Be+t reactions show a maximum at 2 MeV center of mass energy. The cross sections scale directly with the partial width of the resonances, which carry a large uncertainty. The ^{7}Be$(t,\alpha)^{6}$Li reaction should have a comparable strength as the ^{7}Be$(t,^{3}He)^{7}$Li reaction since the strength is determined by the ^{3}He-α cluster structure of the compound states; however, the second reaction is weaker due to the difference in the underlying reaction mechanisms of transfer versus charge exchange, respectively. The ^{7}Be$(t,p)^{9}$Be rate is comparable to the ^{7}Be$(t,n)^{9}$B rate. Another uncertainty comes from possible contributions from particle emission populating higher excited states in the respective final nuclei. The rate for the radiative capture process ^{7}Be$(t,\gamma)^{10}$B is expected to be small in comparison to the particle decay of the resonance states. Overall, the tritium-induced processes seem to be fairly strong, but more detailed experimental studies will be necessary to confirm the present predictions.

4.2.3. Tritium capture on ^{7}Li The cross section of the ^{7}Li$(t,n)^{9}$Be reaction at low energies is characterized by a number of broad resonances associated with highly excited levels including the bound state at 17.12 MeV (2^-), and unbound levels at 17.753 MeV (2^+) and 18.55 MeV (2^-) in ^{10}Be [22, 23] as shown in Fig. 8. The pronounced resonance structure of the cross section also continues towards higher tritium energies [60, 58]. Previous theoretical attempts to describe the observed cross section through interference of direct and resonant reaction mechanisms failed to fit the low-energy data in a satisfactory manner [61]. Recent R-matrix simulations (green line in Fig. 8) provided a reasonable fit for the S-factor data over the energy range near the threshold [24]. This was achieved by suggesting a 2^- resonance at $\approx$17.380 MeV, in addition to the known observed levels. Such an unbound state has not been observed in any other reaction channels and remains experimentally unconfirmed. The quoted resonance parameters are based on the interpretation of the observed high-energy tail within the R-matrix fit. This introduces enormous uncertainties, as already pointed out in an earlier study [23], since resonance parameters have been assumed without specific evidence for such a state in complementary data sets. The low-energy data points might well represent a tail contribution by a lower-energy resonance or even the sub-threshold state at 17.12 MeV. This level has a tentative (2^-) spin parity assignment, based on angular distribution studies of the ^{7}Li(α, p)^{10}Be tritium transfer reaction [62]. The angular distribution data do not exclude a 1^- spin parity assignment. This assignment would suggest that the 17.12 MeV level would be a strong subthreshold state tailing into the tritium unbound range of the excitation curve as demonstrated by the present R matrix simulations indicated by the dash-dotted red line . This tail contribution would cause a significant increase in the reaction rate and would introduce a considerably higher neutron flux in

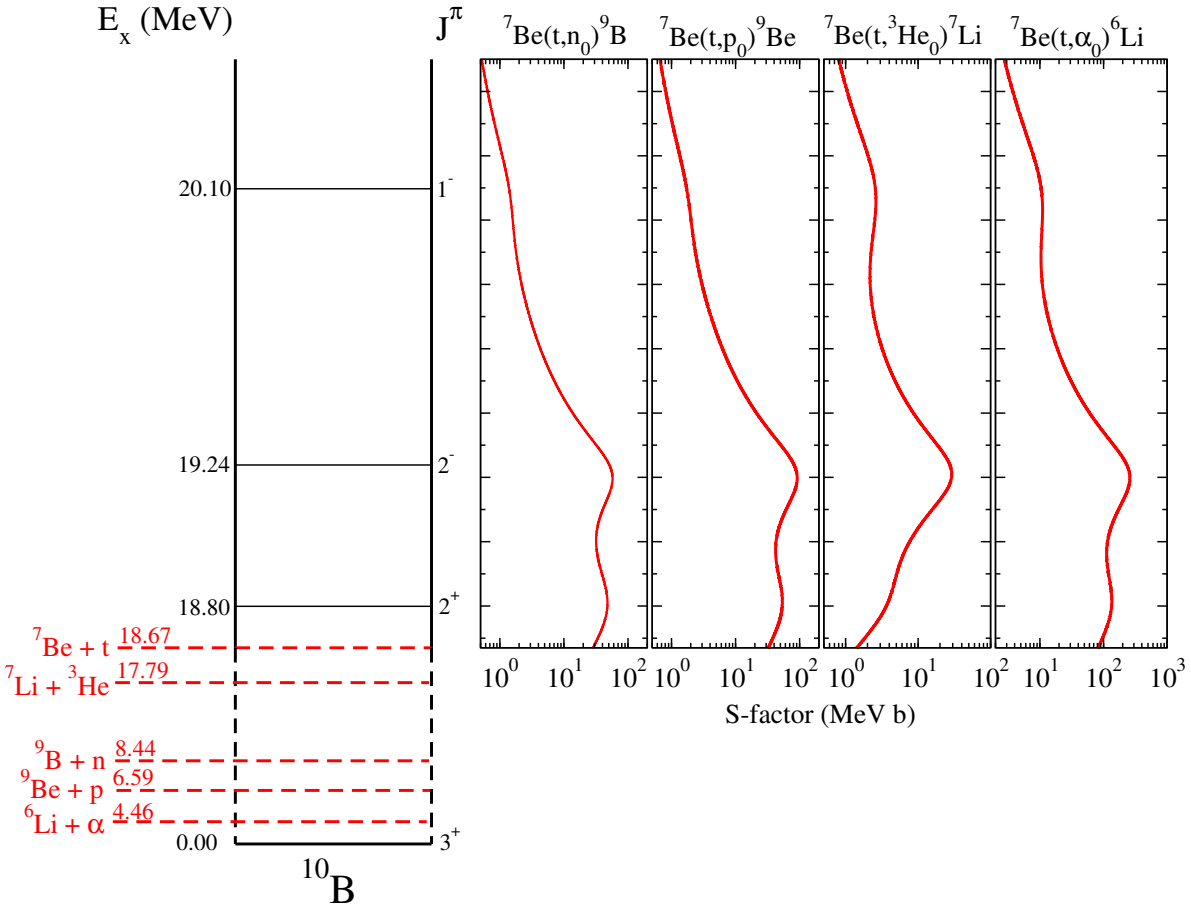

Figure 7. Level scheme of ^{10}B near the tritium separation energy at 18.66 MeV. S-factor curves for the charge exchange reaction ^{7}Be$(t,^3 He)^7$Li and the ^{7}Be$(t,n)^9$B reaction have been calculated on the basis of available resonance data. The reaction channels ^{7}Be$(t,\alpha)^6$Li and ^{7}Be$(t,p)^9$Be are expected to gave comparable strength because of the anticipated nuclear structure features of the compound states.

the burning environment. Fig. 8 shows the level scheme of the ^{10}Be compound nucleus with the possible near-threshold states as well as a R-matrix analysis of the presently existing reaction data. Also shown is the prediction for the HF rate based on the `TALYS` code shown as blue-dashed line . At higher energies the statistical model cross section is clearly larger than the R-matrix predictions, however, toward lower energies the tail of the subthreshold state at 17.12 MeV may become the dominant contribution to the reaction rate. More detailed experimental studies are clearly necessary.

5. Tritium capture on heavy nuclei $A \geq 9$

Tritium-induced reactions on heavier nuclei such as beryllium, boron, carbon, and nitrogen have been studied. The tritium threshold in the compound system is typically very high, and the cross section is characterized by many resonances. Resonance parameters are known only to a limited extent, largely based on transfer reaction

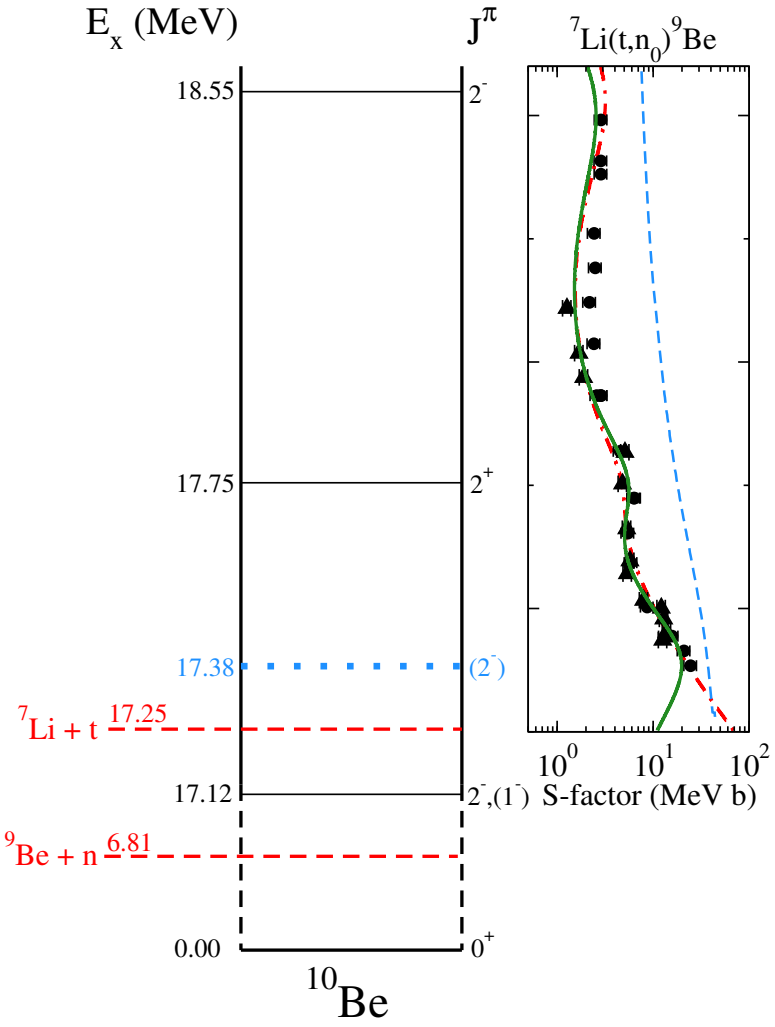

Figure 8. Level scheme of ^{10}Be near the tritium separation energy. S-factor data of the $^{7}\mathrm{Li}(t, n_0)^{9}\mathrm{Be}$ reaction from Brune et al. [22] (black dots) and Barhoumi et al. [23] (black triangles) are compared to R-matrix fits from Hu et al. [24]. This fit relies on the contribution of new 2^- state (blue dotted line in the level scheme) to facilitate a fit matching the data (green line). However tritium transfer reaction studies [62] show no evidence or indication for such a state in the ^{10}Be compound nucleus. The present R-matrix fit of the S-factor date is shown as red dash -dottedline, where the known subthreshold state at $E_x = 17.12$ MeV is changed from $2^- \rightarrow 1^-$ to obtain an alternative fit to the S-factor data without introducing unobserved resonance levels. An estimate of the average ground state S-factor calculated with `TALYS` is shown as blue dashed line.

measurements. S-factor estimates are based on the given level parameters and are compared with statistical model assumptions. The present status of these kind of studies is evaluated in the following analysis.

5.1. Tritium on Beryllium: $^{9}Be(t,\gamma)^{12}B$, $^{9}Be(t,n)^{11}B$, $^{9}Be(t,d)^{10}B$, *and* $^{9}Be(t,\alpha)^{8}Li$

Tritium capture reactions on ^{9}Be populate the compound nucleus ^{12}B above 12.93 MeV. Available experimental data suggest that the level density for tritium-populated resonance states is limited. The cross sections in all observed reaction channels are reported to be devoid of resonance features except the neutron channel, but given the fact that all reaction channels are wide open, the cross section is most likely dominated by contributions from broad and possibly interfering resonance structures located around 13.4 to 14 MeV and possibly some tail contributions from broad bound states at 12.733 MeV [58, 63]. In the low-energy region, the cross sections are described quite well by single resonance Breit-Wigner structures, but at higher energies, broad overlapping resonances dominate the reaction cross sections. Attempts were made in earlier work to describe these cross-sectional data by Hauser-Feshbach calculations; however, angular distribution studies showed rapid changes with energy, suggesting a range of relatively well-separated independent resonances [64]. The energy range near the threshold is not well explored and additional features may contribute. The existing data are limited and not easily available, but R-matrix simulations have been attempted on the basis of the existing resonance information and compared with Hauser-Feshbach calculations using `TALYS` as demonstrated in Fig. 9.

5.2. Tritium on Boron: $^{10,11}B(t,n)^{12,13}C$, $^{10,11}B(t,d)^{11,12}B$, *and* $^{10,11}B(t,\alpha)^{9,10}Be$

Tritium capture on ^{10}B populates the ^{13}C compound system at a very high excitation range above 23.875 MeV. The neutron channel is wide open feeding excited states in ^{12}C. The alpha, deuteron, and proton channels are open as well, and the cross section of all ^{10}B+t reaction channels is expected to be characterized by very broad resonant states.

Tritium capture on ^{11}B populate resonance levels in the ^{14}C compound nucleus above the triton threshold at 20.598 MeV. The level density at this excitation range is not well known and the cross sections of the three reaction channels are expected to be characterized by clusters of broad, possibly interfering resonances in all reaction channels. Resonant structures have been reported in the neutron channel between E_t = 1.20 to 2.32 MeV: These are believed to correspond to ten excited states in ^{14}C in the range $21.54 \leq E_x \leq 22.42$ MeV [65] extending to a tail towards lower energies [58]. Also possible is the $^{11}\mathrm{B}(t,\alpha)^{10}\mathrm{Be}$ reaction channel with a Q-value of 8.585 MeV. However, attempts to measure α-particle as well as the proton and deuteron channels have been unsuccessful [66]. However, transfer reaction studies determined a number of well-separated resonance states at such high excitation energies, which were identified as three-particle cluster configurations [67].

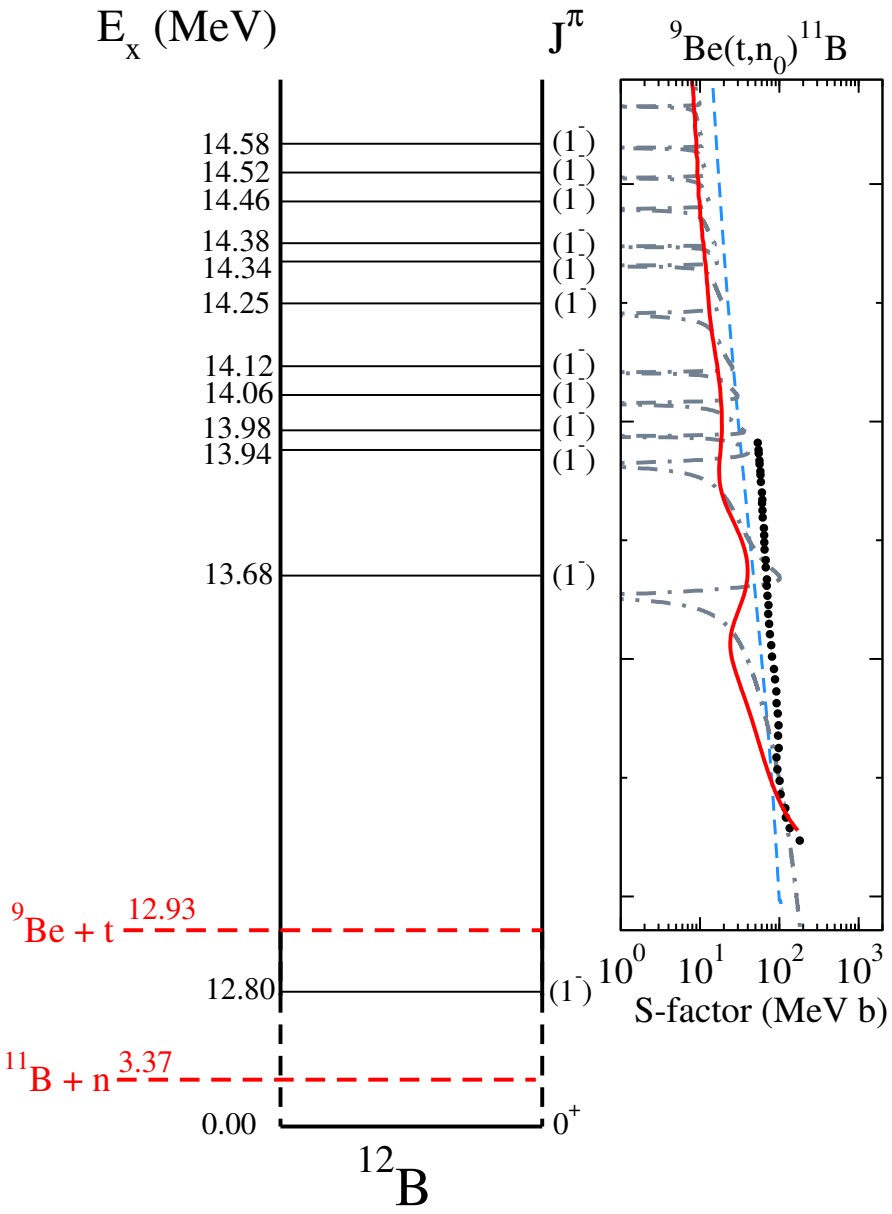

Figure 9. Level scheme of ^{12}B that includes details relevant for the ^{9}Be$(t, n_0)^{11}$B reaction. Energies and widths have been taken from Serov and Guzhovskii [58] in order to make an R-matrix estimate for the upper limit of the S-factor by taking Γ_t and Γ_n to be equal (gray dashed-dotted line). An estimate of the average S-factor has been made using `TALYS` (blue dashed line). The `TALYS` prediction is above the the averaged R-matrix cross section. The calculations are compared to the data of [58], where the red solid line represents the R-matrix calculation convoluted with the experimental resolution of Serov and Guzhovskii [58].

5.3. Tritium on Carbon: $^{12}C(t,n)^{14}N$, $^{12}C(t,p)^{14}C$, *and* $^{12}C(t,\alpha)^{11}B$

Tritium capture on ^{12}C populates resonance levels in the ^{15}N compound nucleus above the triton threshold at 14.85 MeV as shown in Fig. 10. The level density at this excitation range is large and the cross sections of the three reaction channels seem to be characterized by clusters of broad, possibly interfering resonances in all reaction channels [68, 69]. The observed cross sections are dominated by a broad structure slightly above the 2 MeV triton energy in the center-of-mass system corresponding to a region of high-level density between 16 and 17 MeV excitation energy in the compound system ^{15}N [69]. The neutron and proton channels are open, but only direct transfer modes have been studied to probe the shell model configuration of ^{14}N [70]. The experimental data cover a broader energy range between 0.2 and 3 MeV for tritium beam. The deuteron channel is closed at the 15 MeV excitation range in ^{15}N.

An R-matrix calculation has been performed to determine the total ^{12}C+t cross section using the multichannel code `AZURE2`. The cross section prediction is shown as solid red lime and is based on existing reaction data for the different observed exit channels, but also include data on ^{11}B$(\alpha,n)^{14}$N, ^{14}N$(n,p)^{14}$C, ^{14}C$(p,n)^{14}$N, and ^{14}C$(p,p)^{14}$C. The resulting cross section and reaction rate has been compared with Hauser-Feshbach predictions based on the code `TALYS` shown as dashed blue line in Fig. 10.

6. Tritium cluster configurations at the tritium threshold

Tritium capture on higher mass nuclei have not been studied to a great extent except with thick target techniques [72]. The tritium threshold energy is always high, in the 15 to 20 MeV range for the compound system. Typically high excitation energies in a nucleus are associated with high level densities justifying a statistical model approach in deriving the cross sections and reaction rates. These have been calculated using the `TALYS` Hauser-Feshbach code.

On the other hand, the experiments show that tritium cluster configurations emerge at the tritium threshold in the respective compound nucleus. In particular, the reaction cross sections of tritium-induced reactions often seem to be characterized by pronounced single resonances [73, 74] suggesting near-threshold clustering effects [75]. The R-matrix fits and calculations based on tritium transfer data predict in all cases a substantially higher cross section as the comparison of the Hauser-Feshbach predictions demonstrates. While the level density should be high, for most of the states the tritium cluster component will be negligible. Hauser-Feshbach calculations do not include a-priori pronounced cluster configurations, but may represent the contributions of other, non-clusterized level configurations, while the R-matrix calculations reflect the contributions of the observed cluster features, which could be identified through indirect means via tritium transfer reactions.

Near-threshold states provide an interesting opportunity to explore the

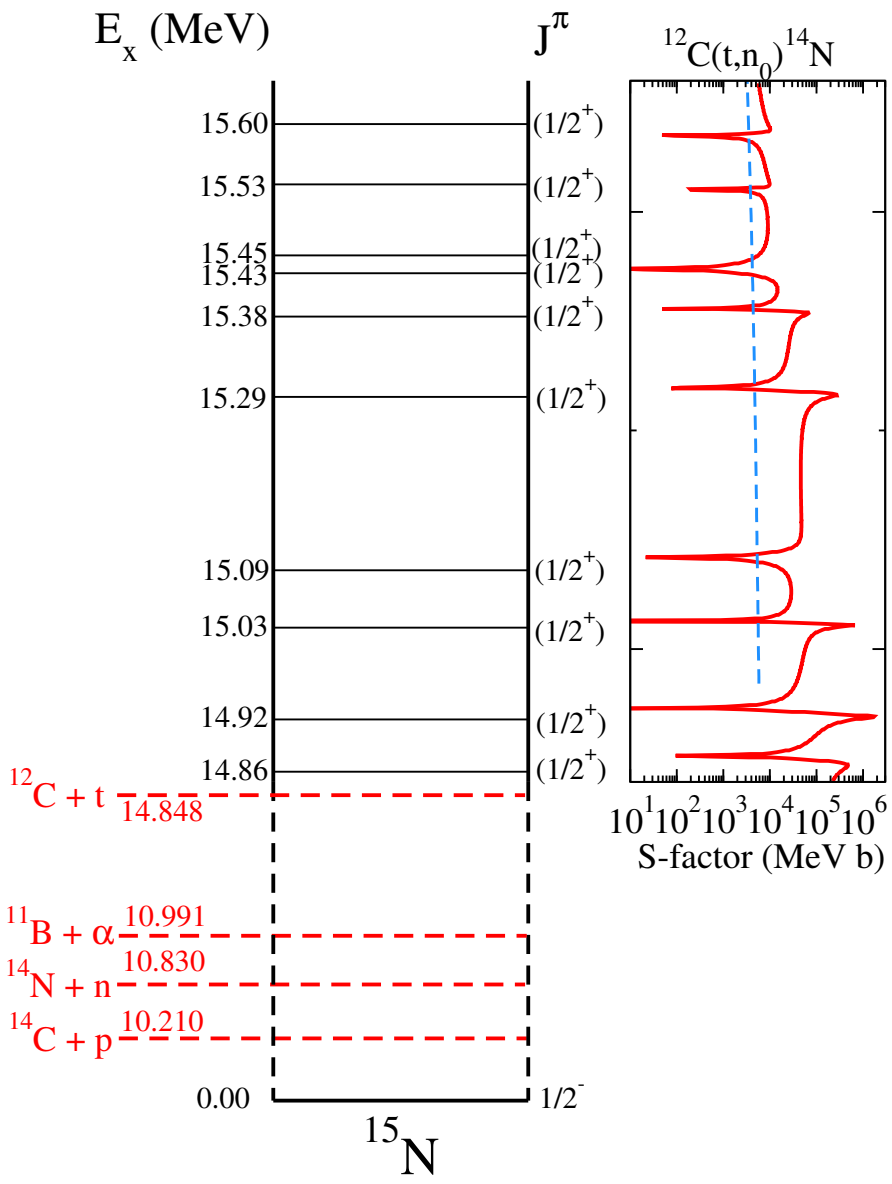

Figure 10. The figure shows the known level structure of the ^{15}N compound nucleus just above the ^{12}C+^{3}H threshold on the left. No data is available at these low energies. The right hand side shows an R-matrix calculation of the cross section (solid red line) based on energy levels and total widths listed in the compilation [71]. As no spin-parity information is known, all levels are taken to be $J^\pi = 1/2^+$ to maximize penetrability and the partial widths are subdivided to maximize the cross section, often with the tritium width equal to the Wigner limit, especially at low energies. The dashed blue line indicates a `TALYS` calculation of the average S-factor.

consequences of threshold effects such as the coupling of bound states with the continuum both in proton and neutron, as well as in alpha capture reactions and can be explained in the framework of the Shell Model Embedded in the Continuum (SMEC) [76]. This novel approach addresses the continuum coupling near the threshold leading to pronounced single-particle configurations in the case of proton and neutron capture reactions, as well as the enhancement of cluster configurations for alpha or, in

this case, tritium capture in light nuclei, which have been treated in the framework of the Gamow-shell model [77, 78].

Despite the high level density at the high excitation energy regime of the tritium threshold, such tritium configurations have been observed in tritium transfer reactions such as (α, p) or $(^7\mathrm{Li}, \alpha)$ populating the tritium cluster configurations in the compound nucleus of the capture reaction [79, 67], as well as in the (t, n), (t, p) and (t, α) decay channels of triton capture reactions [35]. In particular, the (t, n) reactions are of interest, as they provide a neutron release mechanism during a nucleosynthesis event. The (t, α) reactions release high energy α particles, which may generate neutrons via subsequent (α, n) reactions in the surrounding material [80]. Furthermore, tritium-induced reactions, e.g. $^7\mathrm{Li}(t, n)^9\mathrm{Be}$, may trigger (α, n) reactions, e.g. $^9\mathrm{Be}(\alpha, n)$ that serve as secondary neutron sources. This suggests that tritium formed by sequential neutron capture in the early phase of an explosive event at high neutron density may also play an important role in the overall nucleosynthesis budget. Triton-induced reactions are not only able to bridge the mass gap $A = 5$ and 8 without relying on three particle interactions such as the triple-alpha process, but they also serve as neutron storage, releasing neutrons in the subsequent (t, n) reactions or secondary (α, n) reactions boosting neutron production in explosive events. These types of events range from the Big Bang to core collapse supernova and merging neutron stars, influencing rapid nucleosynthesis processes that all emerge from a proton, neutron, and alpha enriched high density environment [81].

While the study of such reactions has been largely neglected, as demonstrated in the present analysis, this work reveals a broad range of experimental opportunities for laser induced plasma experiments [82] which have reached density and temperature conditions sufficiently high to directly probe nuclear processes at stellar burning conditions [83, 84].

7. Experimental opportunities for probing tritium induced reactions on light nuclei

The data on tritium based reactions were mostly obtained at low energy experiments using either tritium beams facilitated at small accelerator laboratories, or alternatively in inverse kinematics experiments using tritium loaded target material being bombarded with heavy ion beam particles. The inverse kinematics experiments are substantially more difficult due to significantly increased security and safety requirements. Unless these direct methods can be redeveloped taking into consideration the formidable safety challenges, other surrogate methods can be utilized to improve the knowledge about tritium level configurations near the threshold. Such alternative methods are tritium transfer reactions such as ^{7}Li,^{9}Be,^{12}C(α, p) or also ^{7}Li,^{9}Be,^{12}C$(^7$Li,$\alpha)$ reactions - to confine ourselves to the previously discussed examples. These reactions can be measured at reasonably high beam energies to populate possible tritium cluster configuration near the threshold region using a magnetic spectrometer to separate the emitted reaction products. Most of the known tritium unbound states discussed in this paper along

with other examples, have been identified and can now be studied in more detail, with higher accuracy using advanced detection and data processing techniques. These studies can be performed at university laboratories with high resolution spectrometers. A complementary approach to identify tritium cluster configurations in higher mass compound nuclei may be inelastic tritium scattering experiments such as ^{15}N (t, t') using the newly available tritium beam at Florida State University [85]. In most cases of states in the vicinity of the tritium threshold, the neutron channel is wide open, suggesting that the tritium unbound states will preferably decay into the neutron channel. This can be studied by complementary neutron-induced reaction or inelastic neutron scattering studies. Such measurements will provide information about the strength of the different decay channels of the triton configurations. Such experiments can be performed with fast neutrons at the LANSCE facility at Los Alamos using recently developed particle detection techniques [86] as well as the n_ToF facility at CERN.

While surrogate studies will provide important information about the high-energy level structure of the nuclei in question, direct measurement can be performed at existing laser plasma facilities, which provide short pulses of high-intensity tritium beams of relatively high intensity during the shot period as demonstrated in Figure 11 which shows the triton spectrum generated at the Omega facility using the Target Normal Sheath Acceleration method [87, 88]. It shows that the tritium flux is constant over the entire low-energy range.

A high tritium flux offers new direct opportunities for the study of tritium-induced reactions at low energies. In order to undertake a reliable analysis of the source and distribution of the neutron flux, it is first necessary to understand the underlying structure of the compound system and possible target impurities. This can be achieved through indirect probing of the associated nuclei, as discussed in the previous section.

8. Tritium based fusion data at plasma facilities

In recent years, several fusion reactions involving tritium and other light nuclei have been studied at laser plasma facilities such as the National Ignition Facility (NIF) [89] and OMEGA [90, 91, 92, 93], and also at the magnetically confined fusion plasma facility JET [94]. This includes studies of ^{3}H+^{3}He; specifically, the cross section for the ^{3}He$(t, \gamma)^6$Li branch was measured [90] and initial measurements of the ^{3}H+^{3}He proton spectrum made [91] at a center-of-mass energy of 80 keV. It also includes measurement of the ^{3}H$(p, \gamma)^4$He cross section [93].

A direct comparison of the laser plasma facility data with that from accelerator-based studies is not straight-forward since at accelerators the reaction yield corresponds to the cross section integrated over the target thickness while at plasma-based experiments the reaction yield corresponds to the reaction rate for the temperature profile of the laser shot. The latter can be approximated by the peak temperature of the plasma; this was done in the comparison of accelerator- and plasma-inferred cross sections in both Zylstra et al. [90] and Mohamed et al. [93].

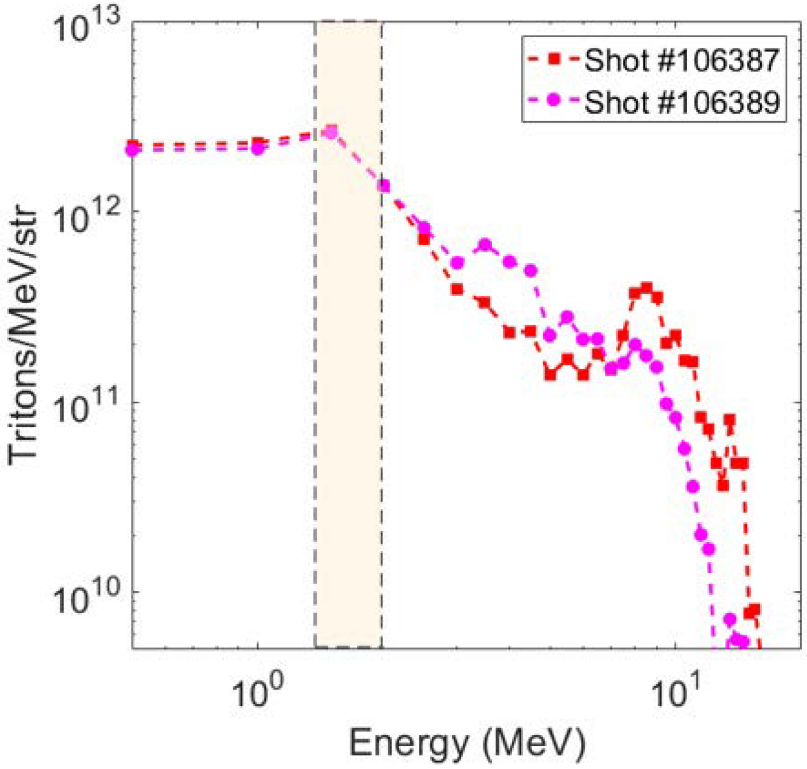

Figure 11. The energy distribution of tritons per MeV and steradian for two shots at the OMEGA facility at the University of Rochester. The energy range corresponding to the peak temperature achieved during the shot is marked by the light yellow band. However towards lower energies the particle flux over the short time period of peak temperature remains remarkably constant in the range of $\approx 2 \cdot 10^{12}$ tritons/MeV/sr.

The ^{3}H+^{3}H reaction studies performed at inertial confinement facilities are limited to the non-resonant $^3\mathrm{H}(t,n)^5\mathrm{He}$ and $^3\mathrm{H}(t,2n)^4\mathrm{He}$ fusion processes. These studies focused on the analysis of the emitted neutron spectra, which contain information about the fusion rate within the temperature range of the plasma between 4-18 keV, corresponding to center-of-mass energies 16-50 keV [94, 92]. As illustrated in Fig. 12 (a), R-matrix analysis applied to the data [96] shows a difference in the relative contribution of the $^3\mathrm{H}(t,n)^5\mathrm{He}$ reaction path to the total number of reactions as a function of center-of-mass energy (red vs black curves); a difference is also seen compared to accelerator measurements [95] at an approximately equivalent c.m. energy of 160 keV (an average value obtained considering stopping of the tritium beam in the target; gray points represent the data, the gray curve an R-matrix fit to the data points). Measurements at OMEGA [92] and the NIF [89, 96] at a similar plasma temperature of 4 keV shown in Fig. 12 (b) demonstrate comparable results (the black curve represents the same R-matrix fit to OMEGA data shown in panel a, the blue data points the neutron spectrum unfolded from NIF data). The low-energy part of the resulting neutron spectra (below 2 MeV) has been poorly constrained in experiments to date; improving upon

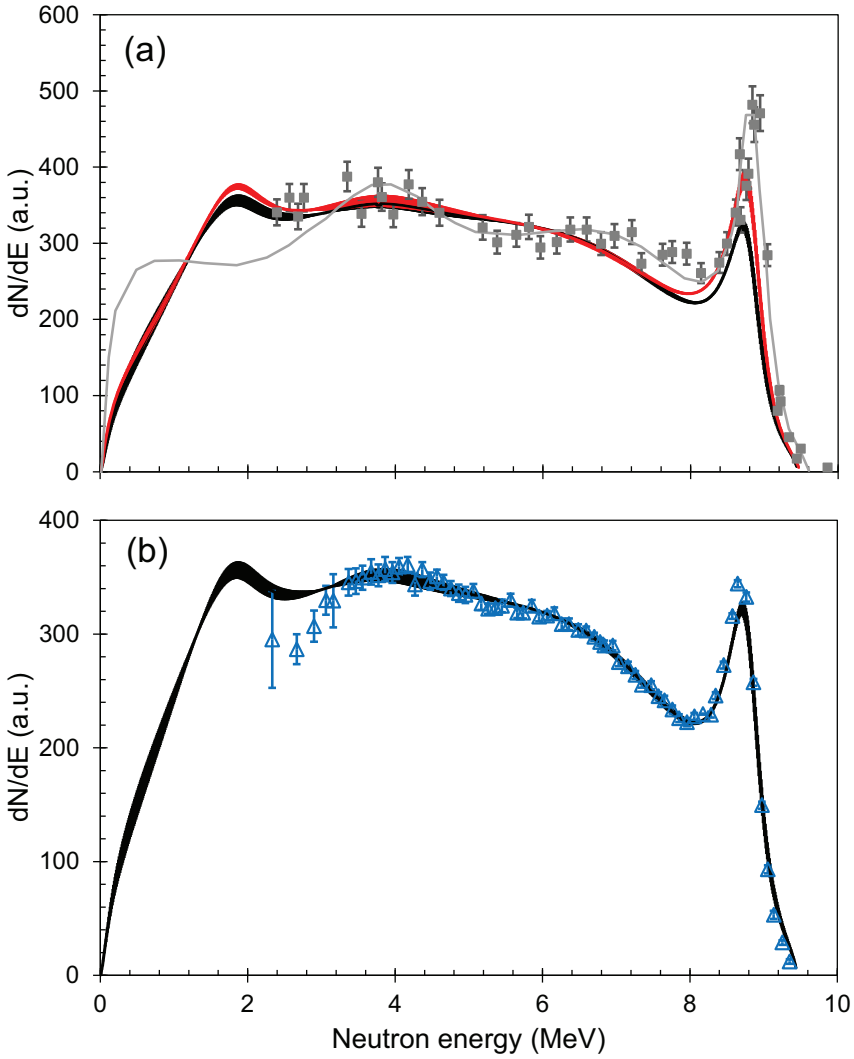

Figure 12. (a) Comparison of R-matrix $T + T$ neutron spectra inferred from fits to measurements at the OMEGA plasma facility at c.m. energies of 16 keV (black) and 50 keV (red), adapted with permission from Ref. [92] copyrighted by the American Physical Society, and from accelerator measurements at 160 keV (gray) [95]. Also shown are the accelerator data (gray points with error bars). The spectra are normalized to their average amplitude in the 4-7 MeV range. The width of the black and red lines represent the estimated systematic uncertainties in the analysis of the OMEGA measurements. (b) Comparison of the 16 keV OMEGA result with data points inferred from a similar measurement at the NIF plasma facility, adapted with permission from Ref. [96] copyrighted by the American Physical Society.

these measurements will better constrain modeling going forward. Tritium capture on higher-mass nuclei has not been performed yet but represents an interesting avenue for future research. More recently, an experiment was performed at the OMEGA facility, generating tritium with an energy distribution centered around 2 MeV interacting with a LiF target resulting in a pronounced neutron flux. The tritium energy distribution also tails towards low energies, covering the whole energy range of interest as shown

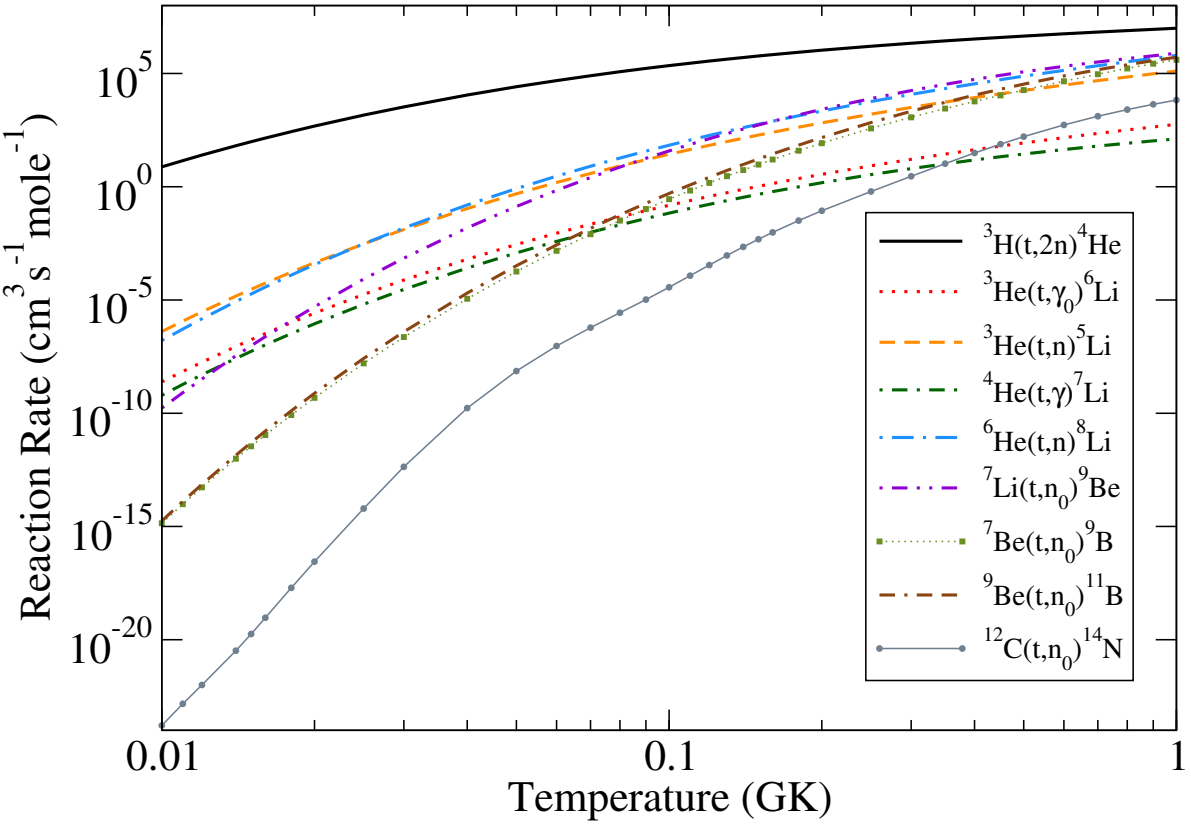

Figure 13. Reaction rates calculated from R-matrix estimates of tritium cross sections discussed in this work.

in Fig. 11 . The neutron flux corresponds to the cross sections of the ^{6}Li$(t,n)^8$Be, ^{7}Li$(t,n)^9$Be, and the ^{19}F$(t,n)^{20}$F reactions, integrated over the energy distribution of the tritium flux. A detailed analysis is still in progress.

9. Reaction rates for tritium induced fusion processes

The reaction yields obtained at plasma facilities corresponds to the reaction rate rather that the cross section. The reaction rate is obtained by integrating the S-factor over the Gamow range of the interacting particles at the temperature T in the stellar core or of a plasma environment as defined in Eq. (5).

The resulting reaction rate is a smooth function exponentially increasing with temperature as can be seen in Fig. 13 which shows the reaction rates of many of the here discussed tritium induced processes as a function of temperature.

The figure demonstrates clearly that the reaction rates are determined by the Coulomb barrier causing the decline towards lower temperatures. However, it should be noted that the reaction rates based on the evaluation of tritium cluster-based resonance states are comparable to the rates anticipated on the basis of the Hauser-Feshbach calculations as shown in Table 1. However, due to the impact of the Coulomb barrier, the reaction rates per mole as presented in Figure 13 are significantly larger than the

Temperature [GK]	^{3}H$(t,2n)$ [RM]	^{3}He(t,γ)	^{6}He(t,n) [RM]	^{7}Li(t,n) [RM]	^{7}Li(t,n) [HF]
0.03	$3.36\times10^{+3}$	7.59×10^{-5}	1.51×10^{-2}	7.0×10^{-4}	3.52×10^{-4}
0.07	$8.0\times10^{+4}$	2.2×10^{-2}	$8.03\times10^{+0}$	$2.54\times10^{+0}$	$2.43\times10^{+0}$
0.1	$2.22\times10^{+5}$	1.52×10^{-1}	$6.81\times10^{+1}$	$3.83\times10^{+1}$	$4.12\times10^{+1}$
0.3	$2.17\times10^{+6}$	$1.65\times10^{+1}$	$1.20\times10^{+4}$	$1.76\times10^{+4}$	$3.16\times10^{+4}$
0.7	$6.75\times10^{+6}$	$2.25\times10^{+2}$	$2.22\times10^{+5}$	$3.32\times10^{+5}$	$9.19\times10^{+5}$
1.0	$9.96\times10^{+6}$	$5.68\times10^{+2}$	$6.27\times10^{+5}$	$7.77\times10^{+5}$	$2.59\times10^{+6}$
Temperature [GK]	^{9}Be(t,n) [RM]	^{9}Be(t,n) [HF]	^{12}C(t,n) [RM]	^{12}C(t,n) [HF]	^{9}Be(α,n)[RM]
0.03	2.66×10^{-8}	1.37×10^{-8}	4.29×10^{-13}	2.24×10^{-17}	5.95×10^{-19}
0.07	1.06×10^{-3}	7.53×10^{-3}	6.03×10^{-7}	1.17×10^{-6}	2.92×10^{-10}
0.1	3.90×10^{-2}	3.01×10^{-1}	3.64×10^{-5}	4.56×10^{-4}	3.93×10^{-7}
0.3	$2.30\times10^{+2}$	$1.47\times10^{+3}$	$3.89\times10^{+0}$	$7.99\times10^{+1}$	6.79×10^{-1}
0.7	$3.36\times10^{+4}$	$1.26\times10^{+5}$	$1.29\times10^{+3}$	$3.97\times10^{+4}$	$5.99\times10^{+2}$
1.0	$2.13\times10^{+5}$	$5.23\times10^{+5}$	$6.70\times10^{+3}$	$2.99\times10^{+5}$	$3.90\times10^{+3}$

Table 1. Reaction rates for tritium induced processes for a temperature range matching laser plasma facility conditions. The rates are calculated on the basis of the presented R-matrix calculations using the code `AZURE2` in comparison to Hauser-Feshbach predictions based on `TALYS` predictions using standard parameters. The Hauser-Feshbach predictions are comparable to the R-matrix calculations which are based on the Wigner limit for calculating the resonance strength. This assumption is based on experimental data from tritium stripping reactions. For comparison the last column shows the reaction rate prediction for the ^{9}Be(α,n) reaction, the strongest known α induced neutron source.

rates for the competing (α,n) reactions as demonstrated on the example of ^{9}Be(α,n). This is not only determined by the Coulomb barrier but also by the strengths of the triton or alpha cluster structure in these light nuclei [97], respectively.

The reaction rates for radiative triton capture (t,γ) processes are typically two to three orders of magnitude lower than the corresponding (t,n) deuteron stripping processes. This is due to the difference between the electromagnetic and the strong interaction Hamiltonian of the reaction process. The consequences are considerable for the (t,n) reactions as potential neutron sources. The tritium-induced rates are considerably larger than the reaction rate for ^{9}Be(α,n), which is by far, the strongest known α-induced neutron source.

10. Conclusion

The reaction rate predictions presented here are based on the publicly available experimental reaction and transfer data. However, the experimental information is incomplete. In particular, the uncertainties from transfer reaction analyses using DWBA calculations [98] are large and can vary within an order of magnitude. In that spirit, we consider the presented R-matrix-based reaction rates as a conservative estimate that needs to be improved. Clearly a new generation of triton experiments is necessary.

A new generation of triton transfer studies would help to explore tritium cluster configurations with improved statistics and resolutions in the higher excitation regions

of the compound nuclei. Such measurements could be expanded beyond the examples listed in this article to nuclei in the higher mass ranges such as ^{18}F and ^{21}Ne for $^{16}\mathrm{O}(t,n)$ and $^{19}\mathrm{F}(t,n)$, respectively. Such studies can be performed at tandem or cyclotron accelerator facilities with (α,p) or also $(^7Li,\alpha)$ triton transfer measurements to explore the population of triton cluster-like configurations above the tritium threshold in compound nuclei for tritium capture reactions. With the installation of high-resolution magnetic spectrographs at the TUNL laboratory at Duke University, the University of Notre Dame, and Florida State University, such studies are feasible to improve the spectroscopy information. Complementary to that the newly developed tritium beam capabilities at FSU will allow for tritium inelastic scattering experiments to probe the levels in question.

This effort can be complemented by direct measurements of tritium-induced reactions using a low-energy tritium beam or a tritium target for inverse kinematic studies. At the present time such studies are handicapped by the lack of accelerated tritium beams; the utilization of tritium targets seems to be a more suitable approach. This approach would have the advantage of allowing for a detailed study of the structure of tritium threshold states.

Conversely, powerful short-pulse laser-ion acceleration mechanisms enable the generation of multi-MeV ion beams with miniaturized targets, which is especially attractive for the creation of radioactive triton beams. The powerful laser systems OMEGA and OMEGA-EP operating at the University of Rochester (UR), and ultimately NSF OPAL are playing an important role in the development of a laser-accelerated triton beam platform with the goal of measuring cross sections of tritium-induced reactions at low energies. An example of a triton beam at the OMEGA Laser Facility is shown in Fig. 11 using the TNSA mechanism.

However, it is widely known that almost all potential application perspectives in laser-driven ion acceleration depend on the production of nearly monoenergetic ion bunches with high beam quality and reliability. Current laser acceleration of electrons, however, are dominated by a rather broad energy spectrum that makes experiments to measure cross-sections much more challenging. Experimental configurations are currently being tested at the UR to increase the purity while reducing the spread in the energy of the emitted ions and generate a more preferential quasi-monoenergetic beam. In addition, as discussed in this paper, the NIF and OMEGA laser facilities allow studies of nuclear reactions involving tritium in implosions, where both reactants follow Maxwellian (or near-Maxwellian) ion velocity distributions.

Finally, very few measurements of these reactions have hitherto been made at any energy, even though tritium-induced reactions occur in all DT plasma thermonuclear fusion research, are critical for an understanding of both stellar and big-bang nucleosynthesis, and, as the lightest nucleus with two neutrons, can serve as a testbed for models of nuclear interactions and structure. Likewise, most of these cross sections have never been measured at the relevant thermonuclear temperatures required for stellar models, yet they are central to understanding the nuclear and astrophysics components

that explain what we observe in the universe.

References

[1] Alain Coc, Stéphane Goriely, Yi Xu, Matthias Saimpert, and Elisabeth Vangioni. Standard Big Bang Nucleosynthesis up to CNO with an Improved Extended Nuclear Network. *The Astrophysical Journal*, 744(2):158, dec 2011. doi: 10.1088/0004-637X/744/2/158. URL https://dx.doi.org/10.1088/0004-637X/744/2/158.

[2] Richard H. Cyburt, Brian D. Fields, Keith A. Olive, and Tsung-Han Yeh. Big bang nucleosynthesis: Present status. *Reviews of Modern Physics*, 88(1):015004, January 2016. doi: 10.1103/RevModPhys.88.015004.

[3] J.M. Lattimer, C.J. Pethick, D.G. Ravenhall, and D.Q. Lamb. Physical properties of hot, dense matter: The general case. *Nuclear Physics A*, 432(3):646–742, 1985. ISSN 0375-9474. doi: https://doi.org/10.1016/0375-9474(85)90006-5. URL https://www.sciencedirect.com/science/article/pii/0375947485900065.

[4] Kohsuke Sumiyoshi, Shun Furusawa, Hiroki Nagakura, Akira Harada, Hajime Togashi, Ken'ichiro Nakazato, and Hideyuki Suzuki. Effects of nuclear matter and composition in core-collapse supernovae and long-term proto-neutron star cooling. *Progress of Theoretical and Experimental Physics*, 2023 (1):013E02, 12 2022. ISSN 2050-3911. doi: 10.1093/ptep/ptac167. URL https://doi.org/10.1093/ptep/ptac167.

[5] N. Thomson, L. Moschini, and A. Diaz-Torres. Laser-assisted deuterium-tritium fusion: A quantum dynamical model. *Phys. Rev. C*, 110:034614, Sep 2024. doi: 10.1103/PhysRevC.110.034614. URL https://link.aps.org/doi/10.1103/PhysRevC.110.034614.

[6] Nelson Jarmie and Ronald E. Brown. Low-Energy nuclear reactions with hydrogen isotopes. *Nuclear Instruments and Methods in Physics Research Section B: Beam Interactions with Materials and Atoms*, 10-11:405–410, 1985. ISSN 0168-583X. doi: https://doi.org/10.1016/0168-583X(85)90279-4. URL https://www.sciencedirect.com/science/article/pii/0168583X85902794.

[7] Y. Xu, K. Takahashi, S. Goriely, M. Arnould, M. Ohta, and H. Utsunomiya. NACRE II: an update of the NACRE compilation of charged-particle-induced thermonuclear reaction rates for nuclei with mass number A<16. *Nuclear Physics A*, 918:61–169, 2013. ISSN 0375-9474. doi: https://doi.org/10.1016/j.nuclphysa.2013.09.007. URL https://www.sciencedirect.com/science/article/pii/S0375947413007409.

[8] Rafael S. de Souza, S. Reece Boston, Alain Coc, and Christian Iliadis. Thermonuclear fusion rates for tritium + deuterium using Bayesian methods. Phys. Rev. C, 99(1):014619, January 2019. doi: 10.1103/PhysRevC.99.014619.

[9] Maria Gatu Johnson, Gerald Hale, Mark Paris, Michael Wiescher, and Alex Zylstra. Editorial: Using high energy density plasmas for nu-

clear experiments relevant to nuclear astrophysics. *Frontiers in Physics*, 11, 2023. ISSN 2296-424X. doi: 10.3389/fphy.2023.1180821. URL https://www.frontiersin.org/articles/10.3389/fphy.2023.1180821.

[10] R. E. Brown and N. Jarmie. Hydrogen Fusion-Energy Reactions. *Radiat.Eff.*, 92: 45, 1986.

[11] S. Typel, G. Blüge, K. Langanke, and W. A. Fowler. Microscopic study of the low-energy ^{3}He(^{3}He, $2p$)^{4}He and ^{3}H(^{3}H, $2n$)^{4}He fusion cross sections. *Z. Physik A - Hadrons and Nuclei*, 339:249–253, 1991. URL https://doi.org/10.1007/BF01284060.

[12] Brian D. Fields. The Primordial Lithium Problem. *Annual Review of Nuclear and Particle Science*, 61(1):47–68, November 2011. doi: 10.1146/annurev-nucl-102010-130445.

[13] G. Beaudet and H. Reeves. Nuclear uncertainties of element yields in the big bang. A&A, 134(2):240–243, May 1984.

[14] P. E. Koehler, C. D. Bowman, F. J. Steinkruger, D. C. Moody, G. M. Hale, J. W. Starner, S. A. Wender, R. C. Haight, P. W. Lisowski, and W. L. Talbert. ^{7}Be(n, p)^{7}Li total cross section from 25 meV to 13.5 keV. Phys. Rev. C, 37(3): 917–926, March 1988. doi: 10.1103/PhysRevC.37.917.

[15] L. Damone, M. Barbagallo, M. Mastromarco, A. Mengoni, L. Cosentino, E. Maugeri, S. Heinitz, D. Schumann, R. Dressler, F. Käppeler, N. Colonna, P. Finocchiaro, J. Andrzejewski, J. Perkowski, A. Gawlik, O. Aberle, S. Altstadt, M. Ayranov, L. Audouin, M. Bacak, J. Balibrea-Correa, J. Ballof, V. Bécares, F. Bečvář, C. Beinrucker, G. Bellia, A. P. Bernardes, E. Berthoumieux, J. Billowes, M. J. G. Borge, D. Bosnar, A. Brown, M. Brugger, M. Busso, M. Caamaño, F. Calviño, M. Calviani, D. Cano-Ott, R. Cardella, A. Casanovas, D. M. Castelluccio, R. Catherall, F. Cerutti, Y. H. Chen, E. Chiaveri, J. G. M. Correia, G. Cortés, M. A. Cortés-Giraldo, S. Cristallo, M. Diakaki, M. Dietz, C. Domingo-Pardo, A. Dorsival, E. Dupont, I. Duran, B. Fernandez-Dominguez, A. Ferrari, P. Ferreira, W. Furman, S. Ganesan, A. García-Rios, S. Gilardoni, T. Glodariu, K. Göbel, I. F. Gonçalves, E. González-Romero, T. D. Goodacre, E. Griesmayer, C. Guerrero, F. Gunsing, H. Harada, T. Heftrich, J. Heyse, D. G. Jenkins, E. Jericha, K. Johnston, Y. Kadi, A. Kalamara, T. Katabuchi, P. Kavrigin, A. Kimura, N. Kivel, U. Köster, M. Kokkoris, M. Krtička, D. Kurtulgil, E. Leal-Cidoncha, C. Lederer-Woods, H. Leeb, J. Lerendegui-Marco, S. Lo Meo, S. J. Lonsdale, R. Losito, D. Macina, J. Marganiec, B. Marsh, T. Martínez, A. Masi, C. Massimi, P. Mastinu, F. Matteucci, A. Mazzone, E. Mendoza, P. M. Milazzo, F. Mingrone, M. Mirea, A. Musumarra, A. Negret, R. Nolte, A. Oprea, N. Patronis, A. Pavlik, L. Piersanti, M. Piscopo, A. Plompen, I. Porras, J. Praena, J. M. Quesada, D. Radeck, K. Rajeev, T. Rauscher, R. Reifarth, A. Riego-Perez, S. Rothe, P. Rout, C. Rubbia, J. Ryan, M. Sabaté-Gilarte, A. Saxena, J. Schell, P. Schillebeeckx, S. Schmidt, P. Sedyshev, C. Seiffert, A. G. Smith, N. V.

Sosnin, A. Stamatopoulos, T. Stora, G. Tagliente, J. L. Tain, A. Tarifeño-Saldivia, L. Tassan-Got, A. Tsinganis, S. Valenta, G. Vannini, V. Variale, P. Vaz, A. Ventura, V. Vlachoudis, R. Vlastou, A. Wallner, S. Warren, M. Weigand, C. Weiß, C. Wolf, P. J. Woods, T. Wright, P. Žugec, and n_TOF Collaboration. ^{7}Be$(n,p)^{7}$Li Reaction and the Cosmological Lithium Problem: Measurement of the Cross Section in a Wide Energy Range at n_TOF at CERN. Phys. Rev. Lett., 121(4):042701, July 2018. doi: 10.1103/PhysRevLett.121.042701.

[16] M. Barbagallo, A. Musumarra, L. Cosentino, E. Maugeri, S. Heinitz, A. Mengoni, R. Dressler, D. Schumann, F. Käppeler, N. Colonna, P. Finocchiaro, M. Ayranov, L. Damone, N. Kivel, O. Aberle, S. Altstadt, J. Andrzejewski, L. Audouin, M. Bacak, J. Balibrea-Correa, S. Barros, V. Bécares, F. Bečvář, C. Beinrucker, E. Berthoumieux, J. Billowes, D. Bosnar, M. Brugger, M. Caamaño, M. Calviani, F. Calviño, D. Cano-Ott, R. Cardella, A. Casanovas, D. M. Castelluccio, F. Cerutti, Y. H. Chen, E. Chiaveri, G. Cortés, M. A. Cortés-Giraldo, S. Cristallo, M. Diakaki, C. Domingo-Pardo, E. Dupont, I. Duran, B. Fernandez-Dominguez, A. Ferrari, P. Ferreira, W. Furman, S. Ganesan, A. García-Rios, A. Gawlik, T. Glodariu, K. Göbel, I. F. Gonçalves, E. González-Romero, E. Griesmayer, C. Guerrero, F. Gunsing, H. Harada, T. Heftrich, J. Heyse, D. G. Jenkins, E. Jericha, T. Katabuchi, P. Kavrigin, A. Kimura, M. Kokkoris, M. Krtička, E. Leal-Cidoncha, J. Lerendegui, C. Lederer, H. Leeb, S. Lo Meo, S. J. Lonsdale, R. Losito, D. Macina, J. Marganiec, T. Martínez, C. Massimi, P. Mastinu, M. Mastromarco, A. Mazzone, E. Mendoza, P. M. Milazzo, F. Mingrone, M. Mirea, S. Montesano, R. Nolte, A. Oprea, A. Pappalardo, N. Patronis, A. Pavlik, J. Perkowski, M. Piscopo, A. Plompen, I. Porras, J. Praena, J. Quesada, K. Rajeev, T. Rauscher, R. Reifarth, A. Riego-Perez, P. Rout, C. Rubbia, J. Ryan, M. Sabate-Gilarte, A. Saxena, P. Schillebeeckx, S. Schmidt, P. Sedyshev, A. G. Smith, A. Stamatopoulos, G. Tagliente, J. L. Tain, A. Tarifeño-Saldivia, L. Tassan-Got, A. Tsinganis, S. Valenta, G. Vannini, V. Variale, P. Vaz, A. Ventura, V. Vlachoudis, R. Vlastou, J. Vollaire, A. Wallner, S. Warren, M. Weigand, C. Weiß, C. Wolf, P. J. Woods, T. Wright, P. Žugec, and n_TOF Collaboration. ^{7}Be$(n,\alpha)^{4}$He Reaction and the Cosmological Lithium Problem: Measurement of the Cross Section in a Wide Energy Range at n_TOF at CERN. Phys. Rev. Lett., 117(15):152701, October 2016. doi: 10.1103/PhysRevLett.117.152701.

[17] Korn, Andreas. The ups and downs of inferred cosmological lithium. *EPJ Web Conf.*, 297:01007, 2024. doi: 10.1051/epjconf/202429701007. URL `https://doi.org/10.1051/epjconf/202429701007`.

[18] Nachiketa Chakraborty, Brian D. Fields, and Keith A. Olive. Resonant destruction as a possible solution to the cosmological lithium problem. *Phys. Rev. D*, 83:063006, Mar 2011. doi: 10.1103/PhysRevD.83.063006. URL `https://link.aps.org/doi/10.1103/PhysRevD.83.063006`.

[19] Nachiketa Chakraborty, Brian D. Fields, and Keith A. Olive. Resonant destruction

as a possible solution to the cosmological lithium problem. Phys. Rev. D, 83(6): 063006, March 2011. doi: 10.1103/PhysRevD.83.063006.

[20] P.D. Forsyth and R.R. Perry. The ^{7}Li(^{3}He, α)^{6}Li reaction between 1.3 and 5.5 MeV. *Nuclear Physics*, 67(3):517–528, 1965. ISSN 0029-5582. doi: https://doi.org/10.1016/0029-5582(65)90544-4. URL https://www.sciencedirect.com/science/article/pii/0029558265905444.

[21] H. Orihara, T. Nakagawa, H. Ueno, T. Tōhei, T. Yamaya, Y. Nakagome, M. Baba, and S. Morita. The (^{3}He, t) reactions on ^{7}Li and ^{9}Be from 2.0 to 4.2 MeV. *Nuclear Physics A*, 139(1):226–240, 1969. ISSN 0375-9474. doi: https://doi.org/10.1016/0375-9474(69)90272-3. URL https://www.sciencedirect.com/science/article/pii/0375947469902723.

[22] C. R. Brune, R. W. Kavanagh, S. E. Kellogg, and T. R. Wang. Cross sections for ^{3}H(^{7}Li,n_0)^{9}Be and ^{3}H(^{7}Li,$n_{\rm tot}$). *Phys. Rev. C*, 43:875–882, Feb 1991. doi: 10.1103/PhysRevC.43.875. URL https://link.aps.org/doi/10.1103/PhysRevC.43.875.

[23] S. Barhoumi, G. Bogaert, A. Coc, P. Aguer, J. Kiener, A. Lefebvre, J.-P. Thibaud, F.M. Baumann, H. Freiesleben, C. Rolfs, and P. Delbourgo-Salvador. Rate of ^{3}H(^{7}Li, n_0)^{9}Be and big-bang nucleosynthesis. *Nuclear Physics A*, 535(1):107–119, 1991. ISSN 0375-9474. doi: https://doi.org/10.1016/0375-9474(91)90518-B. URL https://www.sciencedirect.com/science/article/pii/037594749190518B.

[24] J. Hu, N. Tian, Y. Y. Li, S. Q. Hou, S. W. Xu, J. B. Liu, and J. F. Lv. R-matrix analyses for the ^{7}Li(t, n)^{9}Be and ^{7}Li(^{3}He, p)^{9}Be reactions and their improved thermonuclear reaction rates. *Phys. Rev. C*, 106:045802, Oct 2022. doi: 10.1103/PhysRevC.106.045802. URL https://link.aps.org/doi/10.1103/PhysRevC.106.045802.

[25] A. Koninand S. Hilaire and S. Goriely. TALYS: Modeling of Nuclear Reactions. *Eur. Phys. J.*, 59:131, 2023. doi: 10.1140/epja/s10050-023-01034-3. URL https://link.springer.com/article/10.1140/epja/s10050-023-01034-3.

[26] A. Koning, S. Hilaire, and S. Goriely. Synthesis of the elements within objects exploding from very high temperatures. *Astrophys. J. Suppl.*, 18:247–294, 1969. doi: 10.1086/190191. URL https://doi.org/10.1086/190191.

[27] Hans-Thomas Janka, Florian Hanke, Lorenz Hüdepohl, Andreas Marek, Bernhard Müller, and Martin Obergaulinger. Core-collapse supernovae: Reflections and directions. *Progress of Theoretical and Experimental Physics*, 2012(1): 01A309, 12 2012. ISSN 2050-3911. doi: 10.1093/ptep/pts067. URL https://doi.org/10.1093/ptep/pts067.

[28] Ad.R. Raduta and F. Gulminelli. Nuclear Statistical Equilibrium equation of state for core collapse. *Nuclear Physics A*, 983:252–275, 2019. ISSN 0375-9474. doi: https://doi.org/10.1016/j.nuclphysa.2018.11.003. URL https://www.sciencedirect.com/science/article/pii/S0375947418303816.

[29] J. Görres, H. Herndl, I. J. Thompson, and M. Wiescher. Two-neutron capture reactions in supernovae neutrino bubbles. *Phys. Rev. C*, 52:2231–2235, Oct 1995. doi: 10.1103/PhysRevC.52.2231. URL https://link.aps.org/doi/10.1103/PhysRevC.52.2231.

[30] M. Terasawa, K. Sumiyoshi, T. Kajino, G. J. Mathews, and I. Tanihata. New Nuclear Reaction Flow during r-Process Nucleosynthesis in Supernovae: Critical Role of Light, Neutron-rich Nuclei. *The Astrophysical Journal*, 562(1):470, nov 2001. doi: 10.1086/323526. URL https://dx.doi.org/10.1086/323526.

[31] Amy Bartlett, Joachim Görres, Grant J. Mathews, Kaori Otsuki, Michael Wiescher, Dieter Frekers, Alberto Mengoni, and Jeffrey Tostevin. Two-neutron capture reactions and the r process. *Phys. Rev. C*, 74:015802, Jul 2006. doi: 10.1103/PhysRevC.74.015802. URL https://link.aps.org/doi/10.1103/PhysRevC.74.015802.

[32] M. Hempel, T. Fischer, J. Schaffner-Bielich, and M. Liebendörfer. New Equations of State in Simulations of Core-Collapse Supernovae. *The Astrophysical Journal*, 748(1):70, mar 2012. doi: 10.1088/0004-637X/748/1/70. URL https://dx.doi.org/10.1088/0004-637X/748/1/70.

[33] T. Sasaqui, K. Otsuki, T. Kajino, and G. J. Mathews. Light-Element Reaction Flow and the Conditions for r-Process Nucleosynthesis. ApJ, 645(2):1345–1351, July 2006. doi: 10.1086/504507.

[34] Z. H. Li, W. P. Liu, X. X. Bai, B. Guo, G. Lian, S. Q. Yan, B. X. Wang, S. Zeng, Y. Lu, J. Su, Y. S. Chen, K. S. Wu, N. C. Shu, and T. Kajino. The ^{8}Li$(d,p)^9$Li reaction and the astrophysical ^{8}Li$(n,\gamma)^9$Li reaction rate. *Phys. Rev. C*, 71:052801, May 2005. doi: 10.1103/PhysRevC.71.052801. URL https://link.aps.org/doi/10.1103/PhysRevC.71.052801.

[35] M. Schaeffer, A. Degré, M. Suffert, G. Bonneaud, and I. Linck. Study of the ^{12}C$(t,\gamma_0)^{15}$N reaction around $E_x = 17$ MeV. *Nuclear Physics A*, 275(1):1–12, 1977. ISSN 0375-9474. doi: https://doi.org/10.1016/0375-9474(77)90270-6. URL https://www.sciencedirect.com/science/article/pii/0375947477902706.

[36] K Etoh, T Murata, N Kawai, R Chiba, and S Takayanagi. Triton-Induced Reactions on ^{12}C. *J. Phys. Soc. Jap.*, 26:1335–1344, 1 1969. doi: 10.1143/JPSJ.26.1335. URL https://www.osti.gov/biblio/4758351.

[37] F. Käppeler, R. Gallino, S. Bisterzo, and Wako Aoki. The s-process: Nuclear physics, stellar models, and observations. *Reviews of Modern Physics*, 83(1):157–194, January 2011. doi: 10.1103/RevModPhys.83.157.

[38] John J. Cowan, Christopher Sneden, James E. Lawler, Ani Aprahamian, Michael Wiescher, Karlheinz Langanke, Gabriel Martínez-Pinedo, and Friedrich-Karl Thielemann. Origin of the heaviest elements: The rapid neutron-capture process. *Reviews of Modern Physics*, 93(1):015002, January 2021. doi: 10.1103/RevModPhys.93.015002.

[39] J Bliss, A Arcones, F Montes, and J Pereira. Impact of (α, n) reactions on weak r-process in neutrino-driven winds. *Journal of Physics G: Nuclear and Particle Physics*, 44(5):054003, mar 2017. doi: 10.1088/1361-6471/aa63bd. URL https://dx.doi.org/10.1088/1361-6471/aa63bd.

[40] A. Psaltis, A. Arcones, F. Montes, P. Mohr, C. J. Hansen, M. Jacobi, and H. Schatz. Constraining Nucleosynthesis in Neutrino-driven Winds: Observations, Simulations, and Nuclear Physics. *Astrophys. J.*, 935(1):27, 2022. doi: 10.3847/1538-4357/ac7da7.

[41] V. Vasilevsky, A. V. Nesterov, F. Arickx, and J. Broeckhove. S factor of the ^{3}H(^{3}H,2n)^{4}He and ^{3}He(^{3}He,2p)^{4}He reactions using a three-cluster exit channel. Phys. Rev. C, 63(6):064604, June 2001. doi: 10.1103/PhysRevC.63.064604.

[42] M. Kanafani, X. Fléchard, O. Naviliat-Cuncic, G. D. Chung, S. Leblond, E. Liénard, X. Mougeot, G. Quéméner, A. Simancas Di Filippo, and J.-C. Thomas. High-precision measurement of the ^{6}He half-life. *Phys. Rev. C*, 106:045502, Oct 2022. doi: 10.1103/PhysRevC.106.045502. URL https://link.aps.org/doi/10.1103/PhysRevC.106.045502.

[43] A.M. Govorov, Li Ka-Yeng, G.M. Osetinskii, V.I. Salatskii, and I.V. Sizov. Total Cross Section of the $T + T$ Reaction in the 60 - 1140 keV Energy Range. *Journal of Experimental and Theoretical Physics*, 15(2):266, 1962.

[44] V.I. Serov, S.N. Abramovich, and L.A. Morkin. Total Cross Section Measurement for the Reaction $T(t, 2n)^4$He. *Atomnaya Énergiya*, 42(1):59–61, January 1977.

[45] Nelson Jarmie and Robert C. Allen. $T(t, \alpha)n, n$ Reaction. *Physical Review*, 111(4): 1121–1128, August 1958. doi: 10.1103/PhysRev.111.1121.

[46] S. L. Blatt, A. M. Young, S. C. Ling, K. J. Moon, and C. D. Porterfield. Reaction $T(^3\text{He}, \gamma)^6$Li in the Energy Range 0.5-11 MeV. *Phys. Rev.*, 176:1147–1153, Dec 1968. doi: 10.1103/PhysRev.176.1147. URL https://link.aps.org/doi/10.1103/PhysRev.176.1147.

[47] E. Ventura, C.C. Chang, and W.E. Meyerhof. The ^{3}H(^{3}He,γ)^{6}Li capture reaction and the structure of ^{6}Li. *Nuclear Physics A*, 173(1):1–16, 1971. ISSN 0375-9474. doi: https://doi.org/10.1016/0375-9474(71)90744-5. URL https://www.sciencedirect.com/science/article/pii/0375947471907445.

[48] J. T. Klopcic and S. E. Darden. Cross-Section and Polarization Measurements for the ^{3}H(^{3}He, n)^{5}Li Reaction. *Phys. Rev. C*, 4:1494–1494, Oct 1971. doi: 10.1103/PhysRevC.4.1494. URL https://link.aps.org/doi/10.1103/PhysRevC.4.1494.

[49] C. R. Brune, R. W. Kavanagh, and C. Rolfs. ^{3}H(α,γ)^{7}Li reaction at low energies. Phys. Rev. C, 50(4):2205–2218, October 1994. doi: 10.1103/PhysRevC.50.2205.

[50] Thomas Neff. Microscopic Calculation of the ^{3}He$(\alpha, \gamma)^7$Be and ^{3}H$(\alpha, \gamma)^7$Li Capture Cross Sections Using Realistic Interactions. *Phys. Rev. Lett.*,

106:042502, Jan 2011. doi: 10.1103/PhysRevLett.106.042502. URL https://link.aps.org/doi/10.1103/PhysRevLett.106.042502.

[51] M. Munch, C. Matei, S. D. Pain, M. T. Febbraro, K. A. Chipps, H. J. Karwowski, C. Aa. Diget, A. Pappalardo, S. Chesnevskaya, G. L. Guardo, D. Walter, D. L. Balabanski, F. D. Becchetti, C. R. Brune, K. Y. Chae, J. Frost-Schenk, M. J. Kim, M. S. Kwag, M. La Cognata, D. Lattuada, R. G. Pizzone, G. G. Rapisarda, G. V. Turturica, C. A. Ur, and Y. Xu. Measurement of the ^{7}Li$(\gamma, t)^{4}$He ground-state cross section between E$_\gamma$=4.4 and 10 MeV. Phys. Rev. C, 101(5):055801, May 2020. doi: 10.1103/PhysRevC.101.055801.

[52] T. A. Tombrello, R. J. Spiger, and A. D. Bacher. Deuteron Elastic Scattering from ^{3}He and ^{3}H. *Physical Review*, 154(4):935–940, February 1967. doi: 10.1103/PhysRev.154.935.

[53] J. Pruet, R. D. Hoffman, S. E. Woosley, H. T. Janka, and R. Buras. Nucleosynthesis in Early Supernova Winds. II. The Role of Neutrinos. ApJ, 644(2):1028–1039, June 2006. doi: 10.1086/503891.

[54] C. Fröhlich, G. Martínez-Pinedo, M. Liebendörfer, F. K. Thielemann, E. Bravo, W. R. Hix, K. Langanke, and N. T. Zinner. Neutrino-Induced Nucleosynthesis of $A > 64$ Nuclei: The νp Process. Phys. Rev. Lett., 96(14):142502, April 2006. doi: 10.1103/PhysRevLett.96.142502.

[55] V. Goldberg, B Roeder, Grigor Chubarian, E Johnson, Chaoya fu, A. Alharbi, M. Avila, A. Banu, M McCleskey, J. Mitchell, and Evelynn Simmons. Resonance Scattering to Study Exotic Nuclei at the Limits of Stability. *Journal of Physics: Conference Series*, 337, 02 2012. doi: 10.1088/1742-6596/337/1/012008.

[56] K. Muta, T. Furumoto, T. Ichikawa, and N. Itagaki. Three-triton states in ^{9}Li. *Phys. Rev. C*, 84:034305, Sep 2011. doi: 10.1103/PhysRevC.84.034305. URL https://link.aps.org/doi/10.1103/PhysRevC.84.034305.

[57] W. H. Ma, D. Patel, Y. Y. Yang, J. S. Wang, Y. Kanada-En'yo, R. F. Chen, J. Lubian, Y. L. Ye, Z. H. Yang, Z. Z. Ren, S. Mukherjee, J. B. Ma, S. L. Jin, P. Ma, J. X. Li, Y. S. Song, Q. Hu, Z. Bai, M. R. Huang, X. Q. Liu, Y. J. Zhou, J. Chen, Z. H. Gao, F. F. Duan, S. Y. Jin, S. W. Xu, G. M. Yu, G. Z. Shi, Q. Wang, T. F. Wang, X. Y. Ju, Z. G. Hu, Y. H. Zhang, X. H. Zhou, H. S. Xu, G. Q. Xiao, and W. L. Zhan. Observation of ^{6}He $+ t$ cluster states in ^{9}Li. *Phys. Rev. C*, 103:L061302, Jun 2021. doi: 10.1103/PhysRevC.103.L061302. URL https://link.aps.org/doi/10.1103/PhysRevC.103.L061302.

[58] V. I. Serov and B. Ya. Guzhovskii. Investigation of the reactions ^{6}Li(t, n), ^{7}Li(t, n), ^{7}Li$(^{3}$He$, n)$, ^{9}Be$(t, n)^{11}$B, and ^{9}Be$(^{3}$He$, n)^{11}$C. *The Soviet Journal of Atomic Energy*, 12:1–7, 1962. doi: 10.1007/BF01475993. URL https://doi.org/10.1007/BF01475993.

[59] J.L. Duggan, P.D. Miller, and R.F. Gabbard. A study of the reactions ^{9}Be(^{3}He,n)^{11}C, ^{7}Li(^{3}He,n)^{9}B and ^{13}C(^{3}He,n)^{15}O. *Nuclear Physics*, 46:336–352,

1963. ISSN 0029-5582. doi: https://doi.org/10.1016/0029-5582(63)90604-7. URL https://www.sciencedirect.com/science/article/pii/0029558263906047.

[60] A. K. Val'mer, P. I. Vatset, L. Kolesnikov, S. G. Ya. Tonapetyan, K. K. Chernyavskii, and A. I. Shpetnyi. Neutron yield of the reactions ^{6}Li(t,n) and ^{7}Li(t,n). *he Soviet Journal of Atomic Energy*, 10:574–582, 1962. doi: 10.1007/BF01591264. URL https://doi.org/10.1007/BF01591264.

[61] Y. Yamamoto, T. Kajino, and K.-I. Kubo. Reaction mechanism of ^{7}Li$(^{3}$He$,p)^{9}$Be and ^{7}Li$(^{3}$H$,n)^{9}$Be and primordial nucleosynthesis of ^{9}Be. *Phys. Rev. C*, 47:846–859, Feb 1993. doi: 10.1103/PhysRevC.47.846. URL https://link.aps.org/doi/10.1103/PhysRevC.47.846.

[62] S. Hamada, M. Yasue, S. Kubono, M. H. Tanaka, and R. J. Peterson. Cluster structures in ^{10}Be from the ^{7}Li$(\alpha,p)^{10}$Be reaction. Phys. Rev. C, 49(6):3192–3199, June 1994. doi: 10.1103/PhysRevC.49.3192.

[63] L. N. Generalov, S. N. Abramovich, and A. G. Zvenigorodsk. Total Cross Sections for Neutron Production in Interaction of the Triton with the ^{9}Be Nucleus. *Bull.Rus.Acad.Sci.Phys.*, 65:14, 1 2001. URL http://www-nds.iaea.org/EXFOR/F0525.002.

[64] Krystyna Maluszynska. Study of the ^{9}Be$(t,n)^{11}$B and ^{12}C$(t,n)^{14}$N Reactions at Incident Energies of 1.1 to 1.7 MeV. *ANNALES UNIVERSIT ATIS MARIAE CURIE-SKŁODOWSKA LUBLIN-POLONIA*, 36/37(5):63–73, 1981/1982. URL https://bc.umcs.pl/dlibra/publication/38646/edition/35447/content.

[65] S.G.Tonapetyan P.I.Vatset, L.Y.Kolesnikov. Neutron Emission in Interactions Between Tritons and Boron Nuclei. *Soviet J. Nucl. Phys.*, 1:579, 1965.

[66] F. E. Cecil, R. F. Fahlsing, Nelson Jarmie, R. A. Hardekopf, and R. Martinez. Low-energy ^{7}Li$(t,\alpha)^{6}$He cross sections. *Phys. Rev. C*, 27:6–10, Jan 1983. doi: 10.1103/PhysRevC.27.6. URL https://link.aps.org/doi/10.1103/PhysRevC.27.6.

[67] Z. Y. Tian, Y. L. Ye, Z. H. Li, C. J. Lin, Q. T. Li, Y. C. Ge, J. L. Lou, W. Jiang, J. Li, Z. H. Yang, J. Feng, P. J. Li, J. Chen, Q. Liu, H. L. Zang, B. Yang, Y. Zhang, Z. Q. Chen, Y. Liu, X. H. Sun, J. Ma, H. M. Jia, X. X. Xu, L. Yang, N. R. Ma, and L. J. Sun. Cluster decay of the high-lying excited states in ^{14}C. *Chinese Physics C*, 40(11):111001, 2016. doi: 10.1088/1674-1137/40/11/111001. URL http://hepnp.ihep.ac.cn/en/article/doi/10.1088/1674-1137/40/11/111001.

[68] G. D. Gutsche, H. D. Holmgren, L. M. Cameron, and R. L. Johnston. Differential Cross Sections for Tritium-Induced Reactions on ^{12}C. *Phys. Rev.*, 125:648–655, Jan 1962. doi: 10.1103/PhysRev.125.648. URL https://link.aps.org/doi/10.1103/PhysRev.125.648.

[69] Kiichi Etoh, Tohru Murata, Nawoyuki Kawai, Ren Chiba, and Seiichi Takayanagi. Triton-Induced Reactions on ^{12}C. *Journal of the Physical Society of Japan*, 26(6):1335–1344, 1969. doi: 10.1143/JPSJ.26.1335. URL https://doi.org/10.1143/JPSJ.26.1335.

[70] J.A. Cookson. Spectroscopy of ^{14}N in the ^{12}C(t, n) reaction. *Nuclear Physics A*, 180(1):89–96, 1972. ISSN 0375-9474. doi: https://doi.org/10.1016/0375-9474(72)90158-3. URL https://www.sciencedirect.com/science/article/pii/0375947472901583.

[71] F. Ajzenberg-Selove. Energy levels of light nuclei $A = 13 - 15$. Nucl. Phys. A, 523 (1):1–196, February 1991. doi: 10.1016/0375-9474(91)90446-D.

[72] Nelson Jarmie. Excitation Function of ^{16}O$(t, n)^{18}$F. *Phys. Rev.*, 98:41–42, Apr 1955. doi: 10.1103/PhysRev.98.41. URL https://link.aps.org/doi/10.1103/PhysRev.98.41.

[73] Kiichi Etoh, Nawoyuki Kawai, Yasuhiko Matsuda, and Tohru Murata. Elastic Scattering of Tritons by ^{16}O. *Journal of the Physical Society of Japan*, 24(2):422–422, 1968. doi: 10.1143/JPSJ.24.422. URL https://doi.org/10.1143/JPSJ.24.422.

[74] M. Wery. Elastic scattering of tritons by ^{16}O. *Nuclear Physics A*, 210(2):329–340, 1973. ISSN 0375-9474. doi: https://doi.org/10.1016/0375-9474(73)90306-0. URL https://www.sciencedirect.com/science/article/pii/0375947473903060.

[75] S.N.Abramovich, B.Ya.Guzhovsky, A.V.Ershov, and L.M.Lazarev. Near-Threshold Phenomenon in the Reaction of Light Nuclei. *Izv.Akad.Nauk SSSR, Ser.Fiz.*, 20:2021, 1986. ISSN 0375-9474. doi: https://doi.org/10.1016/0375-9474(73)90306-0. URL https://www.sciencedirect.com/science/article/pii/0375947473903060.

[76] J. Okołowicz, W. Nazarewicz, and M. Płoszajczak. Toward understanding the microscopic origin of nuclear clustering. *Fortschritte der Physik*, 61(2-3):66–79, February 2013. doi: 10.1002/prop.201200127.

[77] Nicolas Michel, Jianguo Li, and Furong Xu. The Gamow shell model with realistic interactions: a theoretical framework for ab initio nuclear structure at drip-lines. *Communications in Theoretical Physics*, 74(9):097303, aug 2022. doi: 10.1088/1572-9494/ac7b19. URL https://dx.doi.org/10.1088/1572-9494/ac7b19.

[78] J. P. Linares Fernandez, N. Michel, M. Płoszajczak, and A. Mercenne. Description of ^{7}Be and ^{7}Li within the Gamow shell model. Phys. Rev. C, 108(4):044616, October 2023. doi: 10.1103/PhysRevC.108.044616.

[79] W Von Oertzen, HG Bohlen, Matko Milin, Tz Kokalova, S Thummerer, Aurora Tumino, R Kalpakchieva, TN Massey, Y Eisermann, G Graw, et al. Search for cluster structure of excited states in ^{14}C. *The European Physical Journal A-Hadrons and Nuclei*, 21:193–215, 2004.

[80] C. Fougères, M. L. Avila, H. Jayatissa, D. Santiago-Gonzalez, K. Brandenburg, Z. Meisel, P. Mohr, F. Montes, C. Müller-Gatermann, D. Neto, W. J. Ong, J. Pereira, K. E. Rehm, T. L. Tang, I. A. Tolstukhin, L. Varriano, G. Wilson, and J. Wu. Direct cross-section measurement of the weak r-process ^{88}Sr(α,n)^{91}Zr reaction in ν-driven winds of core-collapse supernovae. Phys. Rev. C, 109(6):065805, June 2024. doi: 10.1103/PhysRevC.109.065805.

[81] J. Bliss, A. Arcones, F. Montes, and J. Pereira. Impact of (α, n) reactions on weak r-process in neutrino-driven winds. *Journal of Physics G Nuclear Physics*, 44(5): 054003, May 2017. doi: 10.1088/1361-6471/aa63bd.

[82] Ch J Cerjan, L Bernstein, L Berzak Hopkins, R M Bionta, D L Bleuel, J A Caggiano, W S Cassata, C R Brune, D Fittinghoff, J Frenje, M Gatu-Johnson, N Gharibyan, G Grim, Chr Hagmann, A Hamza, R Hatarik, E P Hartouni, E A Henry, H Herrmann, N Izumi, D H Kalantar, H Y Khater, Y Kim, A Kritcher, Yu A Litvinov, F Merrill, K Moody, P Neumayer, A Ratkiewicz, H G Rinderknecht, D Sayre, D Shaughnessy, B Spears, W Stoeffl, R Tommasini, Ch Yeamans, C Velsko, M Wiescher, M Couder, A Zylstra, and D Schneider. Dynamic high energy density plasma environments at the National Ignition Facility for nuclear science research. *Journal of Physics G: Nuclear and Particle Physics*, 45(3):033003, feb 2018. doi: 10.1088/1361-6471/aa8693. URL `https://dx.doi.org/10.1088/1361-6471/aa8693`.

[83] D. T. Casey, Daniel B. Sayre, Carl R. Brune, Vladimir A. Smalyuk, Christopher R. Weber, Robert Eugene Tipton, Jesse E. Pino, G. P. Grim, Bruce A. Remington, David Simon Paul Dearborn, Laura Robin Benedetti, Johan A. Frenje, Maria Gatu-Johnson, Robert Hatarik, N. Izumi, James Mcnaney, T. Ma, G. A. Kyrala, S. A. Maclaren, J. D. Salmonson, S. F. Khan, A. Pak, L Berzak Hopkins, S. Lepape, Brian K. Spears, Nathan B Meezan, Laurent Divol, Charles B. Yeamans, J. A. Caggiano, D. P. McNabb, D. M. Holunga, Marina L. Chiarappa-Zucca, Thomas R. Kohut, and Thomas Gene Parham. Thermonuclear reactions probed at stellar-core conditions with laser-based inertial-confinement fusion. *Nature Physics*, 13:1227 – 1231, 2017. URL `https://api.semanticscholar.org/CorpusID:53497797`.

[84] J. Jeet, A.B. Zylstra, M. Gatu-Johnson, N.V. Kabadi, P. Adrian, C. Forrest, and V. Glebov. Observations of multi-ion physics and kinetic effects in a surrogate to the solar CNO reactions. *High Energy Density Physics*, 49:101066, 10 2023. doi: 10.1016/j.hedp.2023.101066.

[85] Ashton Morelock, Miguel Madurga, Ingo Wiedenhover, Alfredo Galindo-Uribarri, and Augusto Macchiavelli. Updates on the Triton source at Florida State University. In *APS Division of Nuclear Physics Meeting Abstracts*, volume 2024 of *APS Meeting Abstracts*, page J11.001, January 2024.

[86] Hye Lee, S. Mosby, R.C. Haight, and Morgan White. $^{16}\mathrm{O}(n, \alpha)$ cross section investigation using LENZ instrument at LANSCE. *EPJ Web of Conferences*, 122: 05004, 01 2016. doi: 10.1051/epjconf/201612205004.

[87] S. C. Wilks, A. B. Langdon, T. E. Cowan, M. Roth, M. Singh, S. Hatchett, M. H. Key, D. Pennington, A. MacKinnon, and R. A. Snavely. Energetic proton generation in ultra-intense laser–solid interactions. *Physics of Plasmas*, 8(2):542–549, 02 2001. ISSN 1070-664X. doi: 10.1063/1.1333697. URL `https://doi.org/10.1063/1.1333697`.

[88] Andrea Macchi, Marco Borghesi, and Matteo Passoni. Ion accel-

eration by superintense laser-plasma interaction. *Rev. Mod. Phys.*, 85:751–793, May 2013. doi: 10.1103/RevModPhys.85.751. URL https://link.aps.org/doi/10.1103/RevModPhys.85.751.

[89] D. B. Sayre, C. R. Brune, J. A. Caggiano, V. Y. Glebov, R. Hatarik, A. D. Bacher, D. L. Bleuel, D. T. Casey, C. J. Cerjan, M. J. Eckart, R. J. Fortner, J. A. Frenje, S. Friedrich, M. Gatu-Johnson, G. P. Grim, C. Hagmann, J. P. Knauer, J. L. Kline, D. P. McNabb, J. M. McNaney, J. M. Mintz, M. J. Moran, A. Nikroo, T. Phillips, J. E. Pino, B. A. Remington, D. P. Rowley, D. H. Schneider, V. A. Smalyuk, W. Stoeffl, R. E. Tipton, S. V. Weber, and C. B. Yeamans. Measurement of the $T + T$ Neutron Spectrum Using the National Ignition Facility. *Phys. Rev. Lett.*, 111:052501, Aug 2013. doi: 10.1103/PhysRevLett.111.052501. URL https://link.aps.org/doi/10.1103/PhysRevLett.111.052501.

[90] A. B. Zylstra, H. W. Herrmann, M. Gatu Johnson, Y. H. Kim, J. A. Frenje, G. Hale, C. K. Li, M. Rubery, M. Paris, A. Bacher, C. R. Brune, C. Forrest, V. Yu. Glebov, R. Janezic, D. McNabb, A. Nikroo, J. Pino, T. C. Sangster, F. H. Séguin, W. Seka, H. Sio, C. Stoeckl, and R. D. Petrasso. Using Inertial Fusion Implosions to Measure the T+^{3}He Fusion Cross Section at Nucleosynthesis-Relevant Energies. *Phys. Rev. Lett.*, 117:035002, Jul 2016. doi: 10.1103/PhysRevLett.117.035002. URL https://link.aps.org/doi/10.1103/PhysRevLett.117.035002.

[91] A. B. Zylstra, J. A. Frenje, M. Gatu Johnson, G. M. Hale, C. R. Brune, A. Bacher, D. T. Casey, C. K. Li, D. McNabb, M. Paris, R. D. Petrasso, T. C. Sangster, D. B. Sayre, and F. H. Séguin. Proton Spectra from ^{3}He+T and ^{3}He+^{3}He Fusion at Low Center-of-Mass Energy, with Potential Implications for Solar Fusion Cross Sections. *Phys. Rev. Lett.*, 119:222701, Nov 2017. doi: 10.1103/PhysRevLett.119.222701. URL https://link.aps.org/doi/10.1103/PhysRevLett.119.222701.

[92] M. Gatu Johnson, C. J. Forrest, D. B. Sayre, A. Bacher, J.-L. Bourgade, C. R. Brune, J. A. Caggiano, D. T. Casey, J. A. Frenje, V. Yu. Glebov, G. M. Hale, R. Hatarik, H. W. Herrmann, R. Janezic, Y. H. Kim, J. P. Knauer, O. Landoas, D. P. McNabb, M. W. Paris, R. D. Petrasso, J. E. Pino, S. Quaglioni, B. Rosse, J. Sanchez, T. C. Sangster, H. Sio, W. Shmayda, C. Stoeckl, I. Thompson, and A. B. Zylstra. Experimental Evidence of a Variant Neutron Spectrum from the $T(t, 2n)\alpha$ Reaction at Center-of-Mass Energies in the Range of 16–50 keV. *Phys. Rev. Lett.*, 121:042501, Jul 2018. doi: 10.1103/PhysRevLett.121.042501. URL https://link.aps.org/doi/10.1103/PhysRevLett.121.042501.

[93] Z. L. Mohamed, Y. Kim, and J. P. Knauer. Gamma-based nuclear fusion measurements at inertial confinement fusion facilities. *Frontiers in Physics*, 10, 2022. ISSN 2296-424X. doi: 10.3389/fphy.2022.944339. URL https://www.frontiersin.org/journals/physics/articles/10.3389/fphy.2022.944339.

[94] B. Eriksson, S. Conroy, G. Ericsson, J. Eriksson, A. Hjalmarsson, C. R. Brune, M. Gatu Johnson, M. Nocente, S. Fugazza, and M. Rebai. First measurement in a magnetic confinement fusion experiment of the

^{3}H+^{3}H→^{5}He+n intermediate two-body resonant reaction. *Phys. Rev. C*, 109:054620, May 2024. doi: 10.1103/PhysRevC.109.054620. URL https://link.aps.org/doi/10.1103/PhysRevC.109.054620.

[95] C. Wong, J.D. Anderson, and J.W. McClure. Neutron spectrum from the $T + T$ reaction. *Nuclear Physics*, 71(1):106–112, 1965. ISSN 0029-5582. doi: https://doi.org/10.1016/0029-5582(65)90040-4. URL https://www.sciencedirect.com/science/article/pii/0029558265900404.

[96] C. R. Brune, J. A. Caggiano, D. B. Sayre, A. D. Bacher, G. M. Hale, and M. W. Paris. R-matrix description of particle energy spectra produced by low-energy ^{3}H+^{3}H reactions. *Phys. Rev. C*, 92:014003, Jul 2015. doi: 10.1103/PhysRevC.92.014003. URL https://link.aps.org/doi/10.1103/PhysRevC.92.014003.

[97] Martin Freer, Hisashi Horiuchi, Yoshiko Kanada-En'yo, Dean Lee, and Ulf-G. Meißner. Microscopic clustering in light nuclei. *Reviews of Modern Physics*, 90 (3):035004, July 2018. doi: 10.1103/RevModPhys.90.035004.

[98] P. D. Kunz and E. Rost. *The Distorted-Wave Born Approximation*, pages 88–107. Springer New York, New York, NY, 1993. ISBN 978-1-4613-9335-1. doi: 10.1007/978-1-4613-9335-1_5. URL https://doi.org/10.1007/978-1-4613-9335-1_5.